

Noise generation by high-frequency gusts interacting with an airfoil in transonic flow

By I. EVERS AND N. PEAKE

Department of Applied Mathematics and Theoretical Physics, University of Cambridge,
Silver Street, Cambridge CB3 9EW, UK

(Received 5 August 1999 and in revised form 3 December 1999)

The method of matched asymptotic expansions is used to describe the sound generated by the interaction between a short-wavelength gust (reduced frequency k , with $k \gg 1$) and an airfoil with small but non-zero thickness, camber and angle of attack (which are all assumed to be of typical size $O(\delta)$, with $\delta \ll 1$) in transonic flow. The mean-flow Mach number is taken to differ from unity by $O(\delta^{2/3})$, so that the steady flow past the airfoil is determined using the transonic small-disturbance equation. The unsteady analysis is based on a linearization of the Euler equations about the mean flow. High-frequency incident vortical and entropic disturbances are considered, and analogous to the subsonic counterpart of this problem, asymptotic regions around the airfoil highlight the mechanisms that produce sound. Notably, the inner region round the leading edge is of size $O(k^{-1})$, and describes the interaction between the mean-flow gradients and the incident gust and the resulting acoustic waves. We consider the preferred limit in which $k\delta^{2/3} = O(1)$, and calculate the first two terms in the phase of the far-field radiation, while for the directivity we determine the first term ($\delta = 0$), together with all higher-order terms which are at most $O(\delta^{2/3})$ smaller – in fact, this involves no fewer than ten terms, due to the slowly-decaying form of the power series expansion of the steady flow about the leading edge. Particular to transonic flow is the locally subsonic or supersonic region that accounts for the transition between the acoustic field downstream of a source and the possible acoustic field upstream of the source. In the outer region the sound propagation has a geometric-acoustics form and the primary influence of the mean-flow distortion appears in our preferred limit as an $O(1)$ phase term, which is particularly significant in view of the complicated interference between leading- and trailing-edge fields. It is argued that weak mean-flow shocks have an influence on the sound generation that is small relative to the effects of the leading-edge singularity.

1. Introduction

The sound generated by the interaction between convected vortical and entropic disturbances and rotating and stationary blades is a significant component of the total noise emitted by modern aeroengines, and the understanding of the sound generation by gust–blade interaction for a single airfoil is essential for any prediction of turbomachinery noise. The influence of steady-flow distortion due to airfoil thickness, camber and incidence on the noise generation is well-recognised, especially for high-frequency disturbances, and an increasing emphasis is placed on these effects in noise prediction models. Far-reaching analytical results have been achieved for subsonic flow (Myers

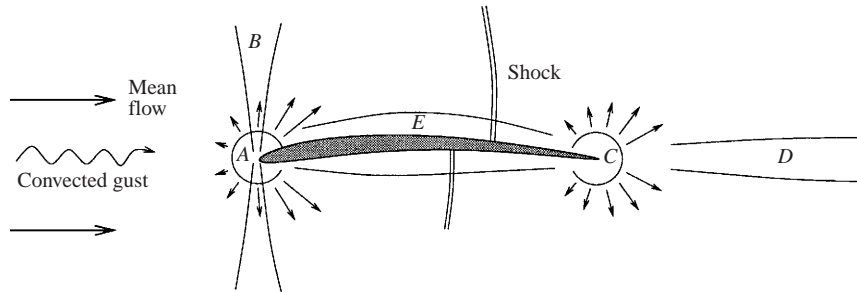


FIGURE 1. Gust-airfoil interaction in transonic flow. The solution will consist of inner asymptotic regions $A-E$ and the outer region (comprising the rest of space).

& Kerschen 1995, 1997; Peake & Kerschen 1997), and here we focus instead on the practically relevant case in which the mean flow around the airfoil is transonic.

Transonic unsteady aerodynamic methods rely largely on numerical codes for nonlinear unsteady flow (Hu & Kandil 1994, and references therein), as well as codes based on a linearization of the Euler equations about a steady mean flow (Verdon & Caspar 1984; Hall, Clark & Lorence 1994). However, numerical approaches encounter difficulties at high frequency, and some results have been achieved analytically using the linearized unsteady transonic small-disturbance equation. Landahl (1989) derives this equation and describes its solution for an isolated airfoil, whereas Surampudi & Adamczyk (1986) consider a two-dimensional cascade of blades, both assuming a uniform mean flow at Mach number equal to one.

In this paper we consider the unsteady flow around a thin cambered airfoil by applying asymptotic methods, in the limit of high reduced frequency k and small camber and thickness (typical size $O(\delta)$, with $\delta \ll 1$), to the Euler equations linearized about the steady transonic small-disturbance (TSD) flow. It mirrors a similar approach used in the subsonic counterpart of this problem by Myers & Kerschen (1995, 1997) and Tsai & Kerschen (1990), who consider the effects of incidence, camber and thickness respectively on gust-airfoil interaction noise. Specifically, we consider the preferred limit in which the free-stream Mach number, M_∞ , differs from unity by $O(\delta^{2/3})$ (standard transonic limit), with $k\delta^{2/3} = O(1)$, which, as will be seen later, will induce an $O(1)$ phase distortion. We believe that Lighthill's (1952) acoustic analogy is not the most appropriate way to address the problem, since the acoustic sources are not compact, but instead we apply the rapid distortion theory put forward by Goldstein (1978), for linear unsteady disturbances to an irrotational compressible steady flow. The distortion of vortical and entropic disturbances by mean-flow gradients is accounted for exactly, while analytical expressions for the volume sources in terms of mean-flow quantities can be found, and the result is an inhomogeneous linear wave equation for an unsteady potential, G , with coefficients that depend on the mean flow. In the limit of large reduced frequency, k , of the incident gust and small mean-flow distortion, with the introduction of the mean-flow potential-streamfunction coordinates (Kerschen & Balsa 1981) and with an incorporation of the perfect-gas thermodynamic relations (Kerschen & Myers 1987), this equation is simplified. The resulting boundary-value problem has a singular perturbation nature, and it turns out that a number of asymptotic regions must be defined (see figure 1).

First, in the inner region A , which scales on the gust wavelength near the leading edge, the gust-airfoil and gust-flow interactions comprise the basic sound production mechanism. The leading-order transonic wave equation predicts singular behaviour of

the unsteady solution directly above and below the leading edge in region B , which we will refer to as the Mach-wave region. The acoustic waves generated in A propagate into the outer region according to a transonic geometric-acoustics formulation, and are rescattered by the airfoil trailing edge in region C , where, in contrast to the leading edge, the mean-flow gradients are not significant and continuity of pressure across the wake now determines the rescattered field. Region C continues into region D along the wake sheet, which provides a transition between the geometric-acoustics fields originating above and below the airfoil. A similar solution also propagates along the airfoil surface in region E , but we will see that in our transonic problem, in contrast to the case of strictly subsonic flow, this region has negligible effect. The results found in each of the above inner regions are matched to a solution in the outer region, thus providing an expression for the total acoustic far field. Here, the presence of possible shock waves and the corresponding interaction with the gust must also be considered, but for the weak shocks found in TSD flow this effect is shown to be smaller than the influence of the mean flow near the leading edge. The aim of all our analysis is to present, in parallel to Myers & Kerschen (1995) for subsonic flow, an asymptotic expression for the far-field noise. We will determine the first two terms in the expansion of the phase, where the second (non-uniform flow) term is $O(k\delta^{2/3}) = O(1)$. In the directivity we will determine all higher terms which are at most $O(\delta^{2/3})$ smaller than the leading-order ($\delta = 0$) directivity. In fact, due to the form of the expansion of the steady flow around the leading edge, we will have to determine ten directivity terms.

In §2, the steady TSD flow about the airfoil is described, including a local approximation of the leading-edge singularity. The equations that govern the unsteady disturbance to this mean flow are formulated in §3, followed in §4 by an examination of the sound generation near the leading edge. Propagation of the acoustic waves is described using a geometric-acoustics formulation in the outer region, as put forward in §5, while the rescattering at the trailing edge and the transition across the wake sheet are considered in §6. The effects of shock waves and of the curvature of the airfoil surface are also discussed in this section. In §7, a numerical study illustrates the effects of gust and mean-flow parameters on the far-field directivity patterns and the total radiated power, and a comparison is made between our transonic theory and the parallel subsonic theory of Myers & Kerschen (1995).

2. Steady flow

We consider a single, two-dimensional airfoil aligned along the x^* -axis from $x^* = 0$ (leading edge) to $x^* = 2b$ (trailing edge). In the coordinate system (x, y) normalized by the airfoil semi-chord b , the profile's upper and lower surfaces are $y = \delta N^\pm(x)$ for $0 \leq x \leq 2$, and are such that the airfoil has $O(\delta)$ thickness, camber and angle of attack with $\delta \ll 1$. The leading edge is parabolic in shape so that

$$N^\pm = \pm(2R)^{1/2}x^{1/2} + s^\pm x + o(x), \quad x \downarrow 0, \quad (2.1)$$

where R is the leading-edge radius non-dimensionalized by $\delta^2 b$ and s^\pm are two constants that depend on the airfoil geometry and angle of attack. The uniform oncoming flow travels in the positive x -direction with velocity $\mathbf{u}_\infty = (U_\infty, 0)$, the upstream Mach number is $M_\infty = U_\infty/a_\infty$, where a_∞ is the upstream speed of sound, and p_∞ , ρ_∞ and S_∞ denote the far-field pressure, density and entropy respectively. The Prandtl–Glauert factor $\beta_\infty^2 = 1 - M_\infty^2$ is small, but may be positive or negative.

We assume that the mean flow is that of an isentropic perfect gas with $S_\infty = 0$,

and that it is described by the normalized steady potential ϕ and streamfunction ψ (both normalized by $U_\infty b$). We write $\phi = x + \phi'$, and for transonic small-disturbance (TSD) flow β_∞^2 and the normalized disturbance potential ϕ' are taken to have the preferred magnitude $O(\delta^{2/3})$. This is rewritten as $\phi' = \delta^{2/3}\varphi'$, where φ' satisfies the TSD equation

$$\left[K - (\gamma + 1) \frac{\partial \varphi'}{\partial x} \right] \frac{\partial^2 \varphi'}{\partial x^2} + \frac{\partial^2 \varphi'}{\partial \tilde{y}^2} = 0, \quad (2.2)$$

with the thin-airfoil boundary condition

$$\frac{\partial \varphi'}{\partial \tilde{y}}(x, 0^\pm) = \frac{dN^\pm}{dx}(x), \quad 0 < x < 2, \quad (2.3)$$

where γ is the ratio of specific heats, the transverse coordinate is stretched to $\tilde{y} = \delta^{1/3}y$, and $K = \beta_\infty^2 M_\infty^{-1} \delta^{-2/3}$ is the transonic similarity parameter (see Cole & Cook 1986). The steady circulation around the airfoil induces a discontinuity in the disturbance potential φ' across the wake, leading to the condition

$$\delta^{2/3}\varphi'(x, 0^+) - \delta^{2/3}\varphi'(x, 0^-) = \Gamma, \quad x \geq 2. \quad (2.4)$$

Here, $U_\infty b \Gamma = O(\delta^{2/3})$ is the circulation, which must be determined as part of the solution. In addition, the steady Kutta condition of smooth velocity at the trailing edge leads to

$$\frac{\partial \varphi'}{\partial x}(2, 0^+) - \frac{\partial \varphi'}{\partial x}(2, 0^-) = 0. \quad (2.5)$$

The arbitrary constant in the definition of φ' is chosen so that φ' disappears at the airfoil leading edge. Following Cole & Cook (1986), the far-field expansion of the disturbance potential can be written as

$$\delta^{2/3}\varphi'(x, \tilde{y}) = -\frac{\Gamma}{2\pi} \tan^{-1} \left(\frac{K^{1/2}\tilde{y}}{x} \right) + \frac{\Gamma}{2} + \phi'(-\infty, 0) + O \left(\frac{\log \tilde{r}}{\tilde{r}} \right), \quad (2.6)$$

where $\tilde{r}^2 = x^2 + K\tilde{y}^2$ and the inverse tangent function jumps from 2π to 0 across the positive x -axis. Equation (2.6) is used in the numerical solution as the far-field boundary condition on the grid boundaries. Of significance to the unsteady analysis to follow is the fact that mean-flow quantities vary slowly with the transverse coordinate y , so that distortion of acoustic and convected waves is dominated by the $O(\delta^{2/3})$ gradients of the mean flow in the streamwise direction.

The boundary-value problem specified by (2.2)–(2.6) for the steady flow can in general only be solved numerically, and we apply the Engquist & Osher (1980) variant of the Murman & Cole (1971) relaxation algorithm (see also Cole & Cook 1986). The algorithm models the TSD equation using eight adaptations of the conventional backward- and centred-difference schemes corresponding to the equal number of possible states of the flow at any given gridpoint, as specified by the criteria formulated by Engquist & Osher (1980); two specify strictly elliptic or hyperbolic behaviour, and the remaining criteria define the behaviour near sonic-line and shock-wave points. The Newton–Raphson method is employed to solve the nonlinear discretized equations for successive columns of the grid, and a single relaxation iteration consists of a sweep across the grid from the column furthest upstream to the column furthest downstream. Local grid refinement leads to improved accuracy, while the application of over-relaxation and under-relaxation at elliptic and hyperbolic points respectively improves convergence. Figure 2 shows the pressure coefficient for a NACA 0006 airfoil

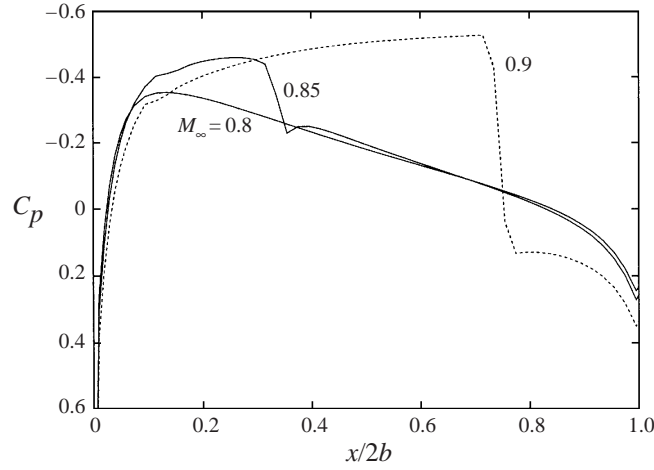


FIGURE 2. Pressure coefficient for a NACA 0006 section at zero angle of attack with varying Mach number.

(6% thickness) at zero angle of attack with $M_\infty = 0.80$, $M_\infty = 0.90$ and $M_\infty = 0.95$; the last two cases have shock waves attached to the upper and lower surfaces.

The primary influence of airfoil geometry and angle of attack on the generation of sound is through the interaction between the (high-frequency) gust and the leading-edge singularity, so the functional form of the steady disturbance potential φ' close to the leading edge is required. In Appendix A, φ' is approximated locally using an approach based on series solutions of the Tricomi equation. Successive exponents of the fractional power series in x are closely spaced, and in order to achieve an accuracy consistent with the approximations to be applied in the unsteady analysis, the series is truncated after 10 terms at $O(|x|)$, leaving

$$\varphi'(x, \tilde{y}) = \sum_{j=0}^9 c_j^\pm (\text{sgn } \tilde{y})^j |x|^{b_j} + O(|x|, |x^{-1/2} \tilde{y}|), \quad (2.7)$$

where the constants c_j^+ and c_j^- correspond to positive and negative x respectively, b_j increases with j and $b_0 = \frac{2}{3}$ (b_9 is the last element in the sequence b_j which is less than unity). The terms in the summation are alternately even and odd in \tilde{y} . Expressions for the constants c_j^\pm and b_j are given in Appendix A.

3. Unsteady flow – formulation

The unsteady flow is taken as an $O(\epsilon)$ perturbation to the mean flow, and we require $0 < \epsilon \ll \delta^{2/3}$ in order to linearize the unsteady flow about the non-uniform mean flow. One physical consequence of this ordering is that the leading-edge stagnation point remains fixed to the asymptotic order considered when the gust is imposed. This approximation would obviously break down for strong vortical forcing. The total local flow speed, velocity, Mach number, speed of sound, pressure, density and entropy are then denoted as $U, \mathbf{u}, M, a, p, \rho$ and S respectively, and we use the same variables with subscript 0 to denote the mean-flow properties, and with a prime to denote the unsteady perturbations to the mean flow; for example, $p = p_0 + \epsilon p' + O(\epsilon^2)$.

We follow Goldstein (1978) and write the unsteady velocity in the form

$$\mathbf{u}' = \nabla G' + \mathbf{v}', \quad (3.1)$$

where \mathbf{v}' contains the vorticity fluctuations (the upstream disturbance as well as vorticity generated further downstream) and G' contains the non-vortical components of the unsteady field including the acoustic waves. Neglecting $O(\epsilon^2)$ terms it turns out that the velocity \mathbf{v}' satisfies a modified form of the linearized momentum equation that can be integrated exactly using the method of characteristics, while the unsteady potential G' satisfies an inhomogeneous wave equation with variable coefficients (see Myers & Kerschen 1995). Although \mathbf{v}' contains the vortical motion of the fluid including the gust at upstream infinity, it is in general not divergence free. However, it represents unsteady motion that is convected with the local mean-flow velocity, so any acoustic motion is represented by G' , which depends on the vortical fluctuations through the rigid-body boundary condition applied on the airfoil surface, and through the source term in the wave equation. The sound propagation is influenced by the mean flow according to the spatial variation of the coefficients on the left-hand side of the wave equation.

As in Myers & Kerschen (1995), it is convenient to convert from physical coordinates (x, y) to the non-dimensional potential-streamfunction coordinates (ϕ, ψ) . The arbitrary constants in ϕ and ψ are chosen such that the leading edge at the origin in (x, y) maps to the origin in (ϕ, ψ) -space. A result of this coordinate transformation is that the boundary condition on the airfoil surface becomes a boundary condition along a section of the ϕ -axis. Since $\phi = x + O(\delta^{2/3})$ and $\psi = y + O(\delta^{2/3})$, we may write $\phi'(x, \tilde{y}) = \phi'(\phi, \tilde{\psi}) + O(\delta^{4/3})$ for the steady perturbation ϕ' to the uniform-flow potential induced by the airfoil, where $\tilde{\psi} = \delta^{1/3}\psi$. As a result of the blade circulation, the trailing edge is mapped onto two points in (ϕ, ψ) -space, with $(2, \pm 0) \rightarrow (\phi_{\text{TE}}^{\pm}, \pm 0)$ and $\phi_{\text{TE}}^+ - \phi_{\text{TE}}^- = \Gamma$. The constants ϕ_{TE}^{\pm} must be determined from the numerical solution of the steady flow.

The incident gust is now introduced by applying a boundary condition at $\phi = -\infty$. Although the airfoil is taken to be two-dimensional, with a geometry and corresponding mean flow independent of the spanwise coordinate, z , the incident gust may have spanwise components. It is assumed that in the reference frame of the airfoil the upstream disturbance can be decomposed into harmonic waves, and consequently we need consider only one such component of frequency ω , namely

$$\left. \begin{aligned} \mathbf{v}' &\sim U_{\infty}(A_t, A_n, A_3)\mathbf{e}^{ik(\phi+k_n\psi+k_3\tilde{z}-\tilde{t})}, \\ s' &\sim 2c_p B\mathbf{e}^{ik(\phi+k_n\psi+k_3\tilde{z}-\tilde{t})}, \quad \phi \rightarrow -\infty, \end{aligned} \right\} \quad (3.2)$$

where $k = \omega b/U_{\infty}$ is the aerodynamic reduced frequency, $\tilde{z} = z/b$ is the non-dimensional spanwise coordinate and \tilde{t} is time normalized by b/U_{∞} . Far upstream, the uniform flow conditions and mass conservation imply that \mathbf{v}' must be divergence free, and hence

$$A_t + A_n k_n + A_3 k_3 = 0. \quad (3.3)$$

Kerschen & Balsa (1981) derived a closed-form expression for \mathbf{v}' that satisfies this upstream boundary condition. For transonic small-disturbance flow, it describes an $O(\delta^{2/3})$ perturbation to the incident plane waves (3.2), except near the leading edge where the mean-flow singularity induces a larger perturbation. Using this expression, the change of variable

$$G'(\phi, \psi, \tilde{z}, \tilde{t}) = U_{\infty} b G(\phi, \psi) \mathbf{e}^{ik(k_3\tilde{z}-\tilde{t})} \mathbf{e}^{ikg_t} \quad (3.4)$$

and the linearized perfect-gas relations, Goldstein’s wave equation becomes

$$\begin{aligned} \frac{\partial^2 G}{\partial \psi^2} + 2ik \frac{\partial G}{\partial \phi} + k^2(1 - k_3^2)G + \left[2ik(\gamma + 1)q - 2ik\beta_\infty^2 - (\gamma + 1) \frac{\partial q}{\partial \phi} \right] \frac{\partial G}{\partial \phi} \\ + \left[k^2(\gamma - 1)q - k^2\beta_\infty^2 + ik(\gamma - 1) \frac{\partial q}{\partial \phi} \right] G + [\beta_\infty^2 - (\gamma + 1)q] \frac{\partial^2 G}{\partial \phi^2} = S(\phi, \psi) e^{ik\chi(\phi, \psi)}, \end{aligned} \quad (3.5)$$

with the source term on the right-hand side given by

$$\begin{aligned} S &= 2ikA_t^* q + 2A_t^* \frac{\partial q}{\partial \phi}, \\ \chi &= \phi + k_n \psi + g(\phi, \tilde{\psi}) - g_l, \\ A_t^* &= A_t - B. \end{aligned}$$

The function $g(\phi, \tilde{\psi})$ is Lighthill’s drift function, and following Myers & Kerschen (1995) this can be approximated by

$$g(\phi, \tilde{\psi}) \sim g_l - 2\phi'(\phi, \tilde{\psi}) \quad (3.6)$$

for a steady potential flow that is a small perturbation to uniform flow. The constant $g_l = g(0, 0) \sim 2\phi'(-\infty, 0)$ is the leading-edge drift, a measure of the phase distortion of waves convecting from upstream to the leading edge, and

$$q = \frac{U_0}{U_\infty} - 1 \sim \frac{\partial \phi'}{\partial \phi} \quad (3.7)$$

is the non-dimensional mean-flow perturbation speed. Near the leading edge, q and g can be approximated using (2.7). The boundary condition of zero normal velocity on the airfoil surface becomes

$$\frac{\partial G}{\partial \psi} = -A_n e^{ik\chi(\phi, 0^\pm)}, \quad \psi = \pm 0, \quad 0 \leq \phi \leq \phi_{TE}^\pm. \quad (3.8)$$

In deriving (3.5) we use the fact that q and its derivatives with respect to ϕ are $O(\delta^{2/3})$, whereas each derivative with respect to ψ is a factor $\delta^{1/3}$ smaller. The most striking difference between (3.5) and its subsonic counterpart is that here the $G_{\phi\phi}$ term is asymptotically small (recall that $q, \beta_\infty^2 = O(\delta^{2/3})$) and will only act as a higher-order forcing term to the $O(1)$ parabolic wave operator in the larger part of the flow domain.

Following the transformation (3.4) it is convenient to also define a modified unsteady pressure \bar{p} according to

$$p'(\phi, \psi, \tilde{z}, \tilde{t}) = \rho_\infty U_\infty^2 \bar{p}(\phi, \psi) e^{ik(k_3 \tilde{z} - \tilde{t})} e^{ikg_l}, \quad (3.9)$$

so that

$$\bar{p} = ikG - \frac{\partial G}{\partial \phi} - q \left(ikG + \frac{\partial G}{\partial \phi} \right). \quad (3.10)$$

In the following sections, we investigate the noise mechanisms in the outer region and in the inner regions referred to in figure 1. On the $O(1)$ scale of the outer region, the high-frequency gust–airfoil interaction can be regarded as inducing point sources near the airfoil edges, and ray fields G_l and G_t emanating from the edges then describe the propagation of the sound through the mean flow. The outer flow also consists of

a particular solution, G_p , that accounts for the distribution of volume sources as given by the source terms of (3.5), and a complementary solution, G_c , that ensures that the boundary condition along the airfoil surface is satisfied. An additional ray field, G_w , that corresponds to inner region D and that renders the trailing-edge scattered field uniformly valid across the wake will also be calculated. In principle, there is also a term, G_s , arising from the interaction between the gust and any steady shocks. We therefore write the total outer solution G_{tot} as

$$G_{\text{tot}} = G_p + G_c + G_l + G_t + G_w + G_s. \quad (3.11)$$

Acoustic waves with amplitudes of order $k^{-3/2}$ and k^{-2} , corresponding to the leading-order terms in the solutions G_l and G_t respectively, will be calculated in the subsequent analysis, along with higher-order terms due to mean-flow effects. The latter will be of order $\delta^{2/3}k^{1-b_j}$ relative to the leading ($\delta = 0$) term in G_l for b_j ranging from $\frac{2}{3}$ to just less than 1, corresponding to the terms in the local expansion of the leading-edge singularity given in (2.7). From this it follows that $\delta^{2/3}k^{1/3} \ll 1$ is a condition required for asymptotic consistency. Indeed, the mean flow near the leading edge is modelled using the thin-airfoil approximation which breaks down in an $O(\delta^2)$ region around the stagnation point, implying that the disturbance wavelength should not be so small as to significantly interact with this local flow. That is, the gust is influenced by the leading-edge singularity but cannot discern the distance between the leading edge and the stagnation point, or alternatively, $\delta^2 \ll 1/k \ll 1$. Amplitude terms of order $\delta^{2/3}$, $\delta k^{1/2}$, $\delta^{4/3}k^{2/3}$ and $1/k$ relative to the leading-order solution are neglected. The terms retained in the phase of the outer solution are of order k , $\delta^{2/3}k$, and here we neglect $O(\delta k)$ terms. Of particular interest is the case $k = O(\delta^{-2/3})$, for which the higher-order phase term is $O(1)$. For an examination of gust–mean flow interaction in the high-frequency TSD regime, this is indeed the preferred scaling relating k and δ , though in all expressions to follow we distinguish between these two independent parameters in order to help clarify which physical mechanisms are represented.

The following calculations for the various asymptotic regions are quite lengthy, and the reader may refer to the beginning of §7 for a summary of the results.

4. Leading-edge region A

We assume that the size of the leading-edge region A scales on the gust wavelength and define the inner variables

$$\Phi = k\phi, \quad \Psi = k\psi, \quad H = kGe^{-i(1-k^2)\Phi/2}, \quad R = kr. \quad (4.1)$$

The local expansions of q and g are substituted in (3.5), resulting in an equation whose leading-order terms define a constant-coefficient linear parabolic operator on H and whose higher-order terms are $O(k^{1-b_j}\delta^{2/3})$ for j ranging from 0 to 9. A correct asymptotic expansion of the solution H is

$$H = H_0 + \sum_{j=0}^9 (H_1^j + H_2^j + H_3^j)\delta^{2/3}k^{1-b_j} + H_4\beta_{\infty}^2, \quad (4.2)$$

where we label the components with subscripts 0 to 4 not only to manage the asymptotics and other mathematical features of the problem, but also to distinguish between the different physical mechanisms that determine those solutions.

4.1. Flat-plate solution H_0

The solution H_0 corresponds to the sound generation by a flat-plate airfoil with semi-infinite chord at zero angle of attack to a uniform oncoming flow of $M_\infty = 1$, and is determined by solving a special case of the boundary-value problem

$$\mathcal{L}(\tilde{H}) \equiv \frac{\partial^2 \tilde{H}}{\partial \Psi^2} + 2i \frac{\partial \tilde{H}}{\partial \Phi} = 0, \quad \left. \frac{\partial \tilde{H}}{\partial \Psi} \right|_{\Psi=0^\pm, \Phi>0} = C(\operatorname{sgn} \Psi)^l \Phi^\alpha e^{iw^2\Phi/2}; \quad (4.3)$$

namely the special case for which $C = -A_n$, $l = 0$ and $\alpha = 0$. Here, l is an integer, $w^2 = 1 + k_3^2$ and we write $\tilde{H}(\Phi, \Psi)$ for the solution of (4.3) that satisfies the radiation condition of out-going waves at infinity. The same boundary-value problem with different values for C , l and α also appears when other components of the inner solution are determined. Note that in this inner region of the potential-streamfunction coordinate system the airfoil upper and lower surfaces lie on the positive Φ -axis with $0 \leq \Phi < \infty$.

The solution \tilde{H} is determined by Fourier transforming (4.3) with respect to Φ and applying the Wiener–Hopf technique, together with the radiation condition and the conditions that the velocity is everywhere continuous and the pressure is everywhere continuous except across the airfoil. The result is

$$\tilde{H}(\Phi, \Psi) = \frac{C\Gamma(\alpha+1)(\operatorname{sgn} \Psi)^{l+1} e^{z\pi i + 3\pi i/4}}{2^{3/2}\pi} \int_{-\infty}^{\infty} \frac{[-i(s - w^2/2)]^{-\alpha-1} e^{a(s, \Phi, \Psi)}}{(-is)^{1/2}} ds, \quad (4.4)$$

where

$$a(s, \Phi, \Psi) = i\Phi s + e^{\pi i/4} |\Psi| (-2is)^{1/2}, \quad (4.5)$$

and where the square-root and other fractional powers of the form z^b , for complex values z and real constants b , are assigned principal values according to $0 \leq \arg(z) < 2\pi$ (i.e. $(-is)^{1/2}$ is discontinuous across the positive imaginary axis in the s -plane). The inversion contour is the real axis deformed below the branch points at $s = 0$ and at $s = w^2/2$. The integrand in (4.4) is analytic in the lower half-plane, and it follows that $\tilde{H} = 0$ for $\Phi < 0$ and $\alpha > -\frac{3}{2}$. The solution therefore predicts zero radiation upstream of the leading edge, as expected in sonic mean flow. We are interested in the behaviour of our inner solution in the outer limit $R \rightarrow \infty$, so we require the outer expansion of (4.4). Standard application of the method of steepest descent reveals that

$$\tilde{H}(\Phi, \Psi) \sim \frac{C\tilde{D}(\theta, \alpha)H(\phi)(\operatorname{sgn} \psi)^{l+1} e^{ik\psi^2/2\phi}}{(k\phi)^{1/2}} \quad \text{as } R \rightarrow \infty, \quad (4.6)$$

where

$$\tilde{D}(\theta, \alpha) = -\frac{(2i)^{\alpha+1} e^{\pi i/4} \Gamma(\alpha+1)}{(2\pi)^{1/2} (\tan^2 \theta + w^2)^{\alpha+1}}, \quad (4.7)$$

$H(\cdot)$ is the unit step function and $\theta = \tan^{-1}(\psi/\phi)$ is the polar angle with $0 \leq \theta < 2\pi$.

When $\alpha = 0$ the expression (4.4) can be evaluated to give the zeroth-order solution H_0 exactly in terms of the complementary error function $\operatorname{erfc}(z)$, specifically

$$H_0(\Phi, \Psi) = \frac{A_n e^{iw^2\Phi/2}}{2w \operatorname{sgn}(\Psi)} \left\{ e^{-w|\Psi|} \operatorname{erfc} \left[\frac{e^{-\pi i/4} (|\Psi| - iw\Phi)}{(2\Phi)^{1/2}} \right] - e^{w|\Psi|} \operatorname{erfc} \left[\frac{e^{-\pi i/4} (|\Psi| + iw\Phi)}{(2\Phi)^{1/2}} \right] \right\}. \quad (4.8)$$

Consistent with (4.6), (4.7) this leads to the outer expansion

$$H_0 \sim \frac{D_0(\theta)H(\phi)e^{ik\psi^2/2\phi}}{(k\phi)^{1/2}}, \quad D_0(\theta) = -A_n \operatorname{sgn}(\Psi)\tilde{D}(\theta, 0). \quad (4.9)$$

For $\Phi \downarrow 0$ (4.8) behaves like $H_0 \sim \Phi^{3/2}\Psi^{-2}e^{i\Psi^2/2\Phi}$, and its derivative with respect to Φ is unbounded and exhibits rapid oscillations. This is the erratic behaviour described in Landahl (1989) that is due to a discontinuity in the strength of the disturbances when cancellation of neighbouring receding waves does not occur. The linearized equation for sonic flow cannot account for these receding waves and therefore predicts a solution that is physically inadmissible near the Φ -axis. Terms that describe a deviation from $M_\infty = 1$ will cancel the singularity and allow the possibility of upstream travelling waves, and this will be presented in §4.5.

4.2. Distortion of the gust: H_1^j

The solutions H_1^j from (4.2) are included to satisfy the inhomogeneous terms in the boundary condition (3.8), which arise when an inner expansion is made of the phase $\chi(\phi, 0^\pm)$ (this involves expanding the drift function near the leading edge, and hence introduces the local series expansion of the steady flow (2.7)). The H_1^j therefore represent the effects of the non-uniform mean flow close to the leading edge on the incident vortical velocity. To determine H_1^j we set $C = 2ic_j^+ A_n$, $l = j$ and $\alpha = b_j$ for $j = 0, \dots, 9$, in (4.3). Using (4.6) we thereby find that the distortion of the gust by the j th component of the local mean flow (2.7) leads to

$$H_1^j \sim \frac{D_1^j(\theta)H(\phi)e^{ik\psi^2/2\phi}}{(k\phi)^{1/2}}, \quad D_1^j(\theta) = 2ic_j^+ A_n (\operatorname{sgn} \psi)^{j+1} \tilde{D}(\theta, b_j), \quad (4.10)$$

as $R \rightarrow \infty$.

4.3. Volume sources: H_2^j

The local solutions H_2^j in (4.2) are included to account for the source term on the right-hand side of (3.5). The equation satisfied by H_2^j is

$$\mathcal{L}(H_2^j) = 2b_j c_j^\pm A_i^* (\operatorname{sgn} \Psi)^j [i|\Phi|^{b_j-1} \operatorname{sgn}(\Phi) + (b_j - 1)|\Phi|^{b_j-2}] e^{iw^2\Phi/2 + ik_n\Psi}, \quad (4.11)$$

with $\partial H_2^j / \partial \Psi = 0$ on $\Psi = 0^\pm$, $\Phi > 0$, where the operator \mathcal{L} is as defined in (4.3). A particular solution, H_{2p}^j , is obtained by taking the double Fourier transform of (4.11), solving for the transform of H_{2p}^j and then inverting back to the ϕ, ψ coordinates. We leave the latter inverse Fourier transform unevaluated in order to simplify subsequent calculations, giving

$$H_{2p}^j(\Phi, \Psi) = - \int_{-\infty}^{\infty} \frac{f(s)ds}{4\pi} \left\{ \frac{e^{ik_n\Psi + i\Phi s} (\operatorname{sgn} \Psi)^j}{s + k_n^2/2 + \epsilon' ik_n \operatorname{sgn}(\Psi)} + e^{a(s, \Phi, \Psi)} \left[\operatorname{sgn}(\Psi) + \frac{e^{\pi i/4} k_n}{(-2is)^{1/2}} \right] \left[\frac{\pi i \delta(s + k_n^2/2)}{\operatorname{sgn}(k_n)} - \frac{H((-1)^{j+1})}{s + k_n^2/2 - \epsilon' ik_n} \right] \right\}, \quad (4.12)$$

where $a(s, \Phi, \Psi)$ is given by (4.5), $\delta(\cdot)$ is the Dirac delta function and

$$f(s) = 2ie^{b_j\pi i} A_i^* \Gamma(b_j + 1) (1 + s - w^2/2) \times \{c^+ [-i(s - w^2/2)]^{-b_j} - c^- [i(s - w^2/2)]^{-b_j}\}. \quad (4.13)$$

The parameter ϵ' in (4.12) is taken in the limit $\epsilon' \downarrow 0$ and is introduced by giving the right-hand side of (4.11) a small artificial decay through an additional factor $e^{-\epsilon'|\Psi|}$ to ensure convergence of the Fourier integrals. In the expression (4.12) it indicates whether the integration contour is indented below or above the pole at $s = -k_n^2/2$, depending on the signs of k_n and Ψ . The far-field expansion of H_{2p}^j consists of three components: the contributions from the branch cuts of the first term inside the curly brackets in (4.12) represent hydrodynamic motion that convects with the mean flow; the branch cuts of the terms involving $H((-1)^{j+1})$ provide the scattering due to the mean-flow discontinuity across $\Psi = 0$ when that component of the mean flow is anti-symmetric about $\Psi = 0$; and the remaining terms involving the delta function plus the various pole contributions represent plane acoustic waves generated across the mean-flow discontinuity at $\Phi = 0$. In that order we find, by applying the method of steepest descent, that

$$\begin{aligned} H_{2p}^j \sim & -\frac{2ib_j c_j^\pm A_l^* |k\phi|^{b_j-1}}{k_n^2 + w^2} (\text{sgn } \phi)(\text{sgn } \psi)^j e^{ikw^2\phi/2 + ikk_n\psi} \\ & + \frac{D_p^j(\theta)H(\phi)e^{ik\psi^2/2\phi}}{(k\phi)^{1/2}} + H(\phi)L_j e^{ik(k_n\psi - k_n^2\phi/2)} \\ & \times \{(-\text{sgn } k_n)^j H(k_n^2 - \tan^2 \theta) + (\text{sgn } \psi)^j H(\tan^2 \theta - k_n^2)\} \end{aligned} \quad (4.14)$$

as $R \rightarrow \infty$, where

$$D_p^j(\theta) = \begin{cases} 0, & j \text{ even} \\ \frac{e^{\pi i/4} 2^{1/2}}{\pi^{1/2}(k_n - \tan \theta)} P_j^+(\theta), & j \text{ odd} \end{cases} \quad (4.15)$$

for $\tan \theta \neq k_n$. Also,

$$P_j^\pm(\theta) = c_j^\pm A_l^* 2^{b_j-1} \Gamma(b_j + 1) e^{\pm b_j \pi i/2} (1 - k_3^2 - \tan^2 \theta) (\tan^2 \theta + w^2)^{-b_j}, \quad (4.16)$$

$L_j = P_j^+(\theta_g) - P_j^-(\theta_g)$, and $\theta_g = \tan^{-1} k_n$ is the gust orientation angle. The first term on the right-hand side of (4.14), the hydrodynamic component, satisfies the non-homogeneous equation (4.11) and does not contribute to the sound field, whereas the other two terms satisfy the homogeneous form of this equation and represent acoustic waves. When θ approaches the gust angle θ_g , it turns out that the saddle point associated with the method of steepest descent approaches the pole $s = -k_n^2/2$ of the integrand in (4.12), so the expansion (4.15) is singular. A uniform expansion of H_{2p}^j cannot satisfy the correct radiation condition because the inner-region equations do not take into account the decay of the volume sources with increasing $|\psi|$ (i.e. the steady-flow expansion (2.7) is independent of $|\tilde{y}|$ in the inner region), and this will necessitate a further treatment of the particular solution in the outer region. Depending on the signs of k_n and Ψ , the pole may or may not be crossed when the integration contour is transformed onto the path of steepest descent, explaining the presence of a phase jump of the plane wave across $\tan \theta = k_n$ when the corresponding component of the mean flow is anti-symmetric. It is apparent from the phase of the third term in (4.14) that the plane-wave disturbances propagate in the direction given by the gust angle θ_g .

The two acoustic components of H_{2p}^j (i.e. the second and third terms in (4.14)) exist downstream of the leading edge only. The scattered field (the second term) exists for odd j only (see (4.15)), and provides the transition that allows for the phase jump of

the plane waves across $\tan \theta = k_n$. We note also that the hydrodynamic component (the first term in (4.14)) has a $|\Phi|^{b_j-1}$ singularity that is stronger than the singularity associated with H_0 , indicating that the asymptotic expansion (4.2) breaks down when $\Phi \rightarrow 0$. By rescaling Φ such that the leading-order expansion of (3.5) includes the $G_{\phi\phi}$ term, a local solution is obtained that is continuous across $\Phi = 0$ and that confirms the presence of this singularity (see Appendix B).

The complementary solution H_{2c}^j that cancels the normal velocity induced by H_{2p}^j consists of a reflected component and a diffracted component. We calculate the far field of the complementary solution directly as follows. The velocity that must be cancelled on $\Psi = 0$ for $\Phi > 0$ is found by differentiating (4.12) under the integral sign and setting $\Psi = 0$. The function $h(s)$ is defined by rewriting the result as

$$\left. \frac{\partial H_{2c}^j}{\partial \Psi} \right|_{\Psi=0} = \frac{-1}{2\pi} \int_{-\infty}^{\infty} h(s) e^{is\Phi} ds \equiv - \left. \frac{\partial H_{2p}^j}{\partial \Psi} \right|_{\Psi=0}. \quad (4.17)$$

The Wiener–Hopf technique followed by the method of steepest descent then gives the outer expansion of H_{2c}^j in the form

$$H_{2c}^j \sim \frac{D_{2c,\text{tot}}^j(\theta) \text{H}(\phi) e^{ik\psi^2/2\phi}}{(k\phi)^{1/2}} - \text{sgn}(k_n\psi) (-\text{sgn} k_n)^j L_j e^{ik(|k_n\psi| - k_n^2\phi/2)} \text{H}(k_n^2 - \tan^2 \theta), \quad (4.18)$$

where

$$D_{2c,\text{tot}}^j(\theta) = - \frac{e^{-\pi i/4} \text{sgn}(\psi)}{(2\pi)^{3/2}} \int_{-\infty}^{\infty} \frac{h(s) ds}{s + \frac{1}{2} \tan^2 \theta + \epsilon' i}. \quad (4.19)$$

The plane waves given by the second term on the right-hand side of (4.18) appear when the deformation of the path of integration of the Fourier inversion integral crosses the pole at $s = -k_n^2/2$. Because the diffraction of the plane-wave component of H_{2p}^j is unbounded at $\theta = \theta_g$ and we anticipate a cancellation of this singularity by components of the trailing-edge field, we isolate the corresponding directivity $D_{2c,\text{sin}}^j$ and write $D_{2c,\text{tot}}^j = D_{2c,\text{sin}}^j + D_{2c}^j$. After considerable calculations and noting that $c_j^- = 0$ for odd j , the results

$$D_{2c}^j(\theta) = \frac{2^{1/2} e^{\pi i/4} k_n (\text{sgn} \psi)^{j+1}}{\pi^{1/2} (k_n^2 - \tan^2 \theta)} [P_j^+(\theta) - P_j^+(\theta_g)] + \frac{2^{1/2} e^{\pi i/4}}{\pi^{1/2} (k_n^2 - \tan^2 \theta)} [2k_n \text{H}(k_n\psi) P_j^+(\theta_g) - (\tan \theta + k_n) P_j^+(\theta)]_{j \text{ odd}} \quad (4.20)$$

and

$$D_{2c,\text{sin}}^j = - \frac{2^{1/2} k_n L_j e^{\pi i/4} (-\text{sgn} k_n)^j \text{sgn}(\psi)}{\pi^{1/2} (\tan^2 \theta - k_n^2)} \quad (4.21)$$

are found. The first term on the right-hand side of (4.20) represents the diffraction of the hydrodynamic component of H_{2p}^j and the second term is the diffraction of the D_p^j component of H_{2p}^j . Both terms are well-behaved for θ near θ_g . The local analysis here predicts a singularity in $D_{2c,\text{sin}}^j$ because in the inner region the airfoil chord is infinite, and no account is therefore taken of the fact that the plane waves are reflected over

only a finite chord. This singularity will be removed by including the effects of the trailing edge in § 5.4.

4.4. Distortion of the acoustic field: H_3^j

The solutions H_3^j in (4.2) represent the influence of the variable-property steady medium on the acoustic propagation, and involve the terms on the left-hand side of (3.5) that depend on q . The problem is

$$\begin{aligned} \mathcal{L}(H_3^j) = (\gamma + 1)c_j^+ b_j (\text{sgn } \Psi)^j \Phi^{b_j-2} & \left\{ \Phi \frac{\partial^2 H_0}{\partial \Phi^2} + [(b_j - 1) - iw^2 \Phi] \frac{\partial H_0}{\partial \Phi} \right. \\ & \left. + \left[\frac{2\Phi}{(\gamma + 1)} + \frac{2i(b_j - 1)}{(\gamma + 1)} - \frac{iw^2(b_j - 1)}{2} - \frac{w^4 \Phi}{4} \right] H_0 \right\}, \end{aligned} \quad (4.22)$$

with again $\partial H_3^j / \partial \Psi = 0$ along the positive Φ -axis. Using the fact that the right-hand side of (4.22) comprises products of solutions of $\mathcal{L}(H) = 0$ and functions of Φ , a particular solution H_{3p}^j is obtained by integrating those functions of Φ and multiplying by $-i/2$. By evaluating the derivatives of H_0 using (4.8), the result is simplified to

$$\begin{aligned} H_{3p}^j = c^+ (\text{sgn } \Psi)^j \Phi^{b_j-1} (b_j - i\Phi) H_0 - \frac{(\gamma + 1)c^+ e^{\pi i/4} A_n (\text{sgn } \Psi)^{j+1}}{4(2\pi)^{1/2}} \\ \times [w^2 \Phi + (2b_j - 1)i + \Psi^2 / \Phi] H(\Phi) \Phi^{b_j-3/2} e^{i\Psi^2/2\Phi}. \end{aligned} \quad (4.23)$$

A complication has been introduced by the fact that H_{3p}^j is more singular than H_0 in the limit $R \downarrow 0$ for the values of b_j considered; the former behaves like $R^{b_j-3/2}$ while from (4.8) the latter behaves like $R^{1/2}$ (recall that $b_j < 1$ for the leading-order terms considered). This implies that the asymptotic expansion (4.2) breaks down sufficiently close to the leading edge, and it corresponds to the last term on the left-hand side of (3.5) being of order of magnitude greater than or equal to that of the first. When the singularity in H_{3p}^j is of degree $b_j - \frac{1}{2}$ or weaker, there is no inconsistency and it merely signifies the existence of another asymptotic region. On the other hand, if the singularity is any stronger, the series (4.2) breaks down even at R of order greater than that for which the expansion of (3.5) breaks down. The singularity in H_{3p}^j is therefore mathematically inadmissible, represents unphysical behaviour and must be cancelled by an eigensolution H_{3e}^j . In Appendix B, this eigensolution is derived by an analysis of the above-mentioned asymptotic region that includes the limit $R \downarrow 0$. The scaling that gives the greatest overlap and that is chosen in the Appendix is one for which Φ is small and of an order that depends on b_j , while Ψ^2 / Φ is kept $O(1)$. Rather than calling this inner region within the leading-edge region A the ‘inner-inner region’, it will be referred to as the ‘Mach-wave region’ or region B . The result of the Mach-wave region analysis is that the eigenfunction which must be introduced in order to cancel the unphysical singularity in H_{3p}^j is

$$H_{3e}^j(\Phi, \Psi) = E_j (\text{sgn } \Psi)^{j+1} \Phi^{b_j-3/2} M\left(\frac{3}{2} - b_j, \frac{1}{2}, i\Psi^2/2\Phi\right) H(\Phi), \quad (4.24)$$

where M is Kummer’s confluent hypergeometric function, and

$$E_j = \frac{(\gamma + 1)c^+ e^{-\pi i/4} A_n (1 - 2b_j)}{4(2\pi)^{1/2}}. \quad (4.25)$$

The final component of H_3^j is the complementary solution H_{3c}^j that ensures that the

velocity

$$\left. \frac{\partial H_{3p}^j}{\partial \Psi} \right|_{\Psi=0} = A_n c^+ (\operatorname{sgn} \Psi)^j (i\Phi^{b_j} - b_j \Phi^{b_j-1}) e^{iw^2\Phi/2} \quad (4.26)$$

of the particular solution is cancelled on the airfoil surface. It is determined by substituting the appropriate values $C = iA_n c^+$, $l = j$, $\alpha = b_j$ (the first term in (4.26)) and $C = -b_j A_n c^+$, $l = j$, $\alpha = b_j - 1$ (the second term in (4.26)) in the boundary-value problem (4.3). Consequently, the solution H_3^j is $H_3^j = H_{3p}^j + H_{3e}^j + H_{3c}^j$, and applying standard results for the far-field expansion of (4.24) (see Abramowitz & Stegun 1972) and (4.6), (4.7) for the far-field expansion of H_{3c}^j , we find that

$$H_3^j \sim \frac{D_3^j(\theta) H(\phi) e^{ik\psi^2/2\phi}}{(k\phi)^{1/2}} + \frac{H(\phi) (\operatorname{sgn} \psi)^j i c_j^+ D_0(\theta) e^{ik\psi^2/2\phi}}{8(k\phi)^{1/2-b_j}} [(\gamma+1)(\tan^2 \theta + w^2)^2 - 8], \quad (4.27)$$

as $R \rightarrow \infty$, where

$$D_3^j(\theta) = A_n (\operatorname{sgn} \psi)^{j+1} c_j^+ [b_j \tilde{D}(\theta, b_j - 1) - i \tilde{D}(\theta, b_j)] + \frac{i 2^{b_j-1} (\operatorname{sgn} \psi)^{j+1} E_j e^{-b_j \pi i/2} \pi^{1/2}}{\Gamma(\frac{3}{2} - b_j) |\tan \theta|^{2b_j-2}}. \quad (4.28)$$

The second term on the right-hand side of (4.27) behaves like $r^{b_j-1/2}$ in the limit $r \rightarrow \infty$, does not represent additional sound generation, and will be matched with phase terms of the leading-edge ray field in the outer region. By contrast, the first term in (4.27) represents sound generation due to the interaction between H_0 , the mean flow and the airfoil. In (4.28) we distinguish the diffraction of the particular solution (first term) from the acoustic field generated by the H_0 -mean flow interaction directly (second term). The former is derived from the complementary solution H_{3c}^j and is symmetric in ψ when j is even, while the latter is the outer expansion of H_{3e}^j and is symmetric when j is odd.

4.5. Variable oncoming-flow speed: H_4

The final component of the inner solution (4.2) describes the influence of the deviation of the upstream Mach number from one, and satisfies the boundary value problem

$$\mathcal{L}(H_4) = -\frac{\partial^2 H_0}{\partial \Phi^2} + iw^2 \frac{\partial H_0}{\partial \Phi} + \frac{w^4}{4} H_0, \quad \left. \frac{\partial H_4}{\partial \Psi} \right|_{\Psi=0} = 0. \quad (4.29)$$

A particular solution is obtained by multiplying the right-hand side of (4.29) by $-i\Phi/2$, and we find that the result

$$H_{4p}(\Phi, \Psi) = \frac{A_n e^{-\pi i/4}}{4(2\pi)^{1/2}} \operatorname{sgn}(\Psi) H(\phi) \Phi^{-1/2} e^{i\Psi^2/2\phi} - \frac{i D_0(\theta)}{8} (\tan^2 \theta + w^2)^2 H(\phi) \Phi^{1/2} e^{i\Psi^2/2\phi} \quad (4.30)$$

already satisfies the boundary condition. As encountered in the calculations for H_3 , there is an inadmissible singularity in H_{4p} near the leading edge and an eigensolution must be included. Again, equation (3.5) is rescaled to the Mach-wave region defined here by the inner variables $\xi = \Phi/\beta_\infty^2$, $\eta = \Psi/\beta_\infty$, resulting in the boundary-value

problem

$$\frac{\partial^2 \mathcal{G}}{\partial \xi^2} + \frac{\partial^2 \mathcal{G}}{\partial \eta^2} + 2i \frac{\partial \mathcal{G}}{\partial \xi} = 0, \quad \left. \frac{\partial \mathcal{G}}{\partial \eta} \right|_{\eta=0^\pm, \xi>0} = -\frac{A_n \beta_\infty}{k}, \quad (4.31)$$

where \mathcal{G} is the unsteady potential G in the Mach-wave region. Using the Wiener–Hopf technique, this problem is solved exactly to give

$$\mathcal{G}(\xi, \eta) = \frac{A_n \beta_\infty \operatorname{sgn}(\eta)}{k} \left\{ \pi^{-1/2} e^{\pi i/4} (\rho + \xi)^{1/2} e^{i(\rho - \xi)} - |\eta| \operatorname{erfc} [e^{-\pi i/4} (\rho - \xi)^{1/2}] \right\}, \quad (4.32)$$

where $\rho^2 = \xi^2 + \eta^2$. The matching between (4.30) and (4.32) is consistent if we include an additional eigensolution that cancels the first term on the right-hand side of (4.30); indeed, this term is a special case of the eigensolution (B 7), namely that for which $A = \tau = C_2 = 0$ and $b = 1$. The other part of (4.30) is singular for $R \rightarrow \infty$ and matches with terms of the inner expansion of the leading-edge ray field, and we therefore conclude that the deviation of the oncoming flow from $M_\infty = 1$ does not result in additional sound waves.

Of related interest is the approximation of \mathcal{G} at large distances from the leading edge found by expanding (4.32) for large ρ and writing the result in coordinates ϕ and ψ :

$$\begin{aligned} \mathcal{G} \sim & -\frac{A_n e^{-\pi i/4} \beta_\infty^2}{2\pi^{1/2} \operatorname{sgn}(\psi) k^{3/2}} \\ & \times \frac{[(1 + \beta_\infty^2 \tan^2 \theta)^{1/2} + \operatorname{sgn}(\phi)]^{1/2}}{|\phi|^{1/2} [(1 + \beta_\infty^2 \tan^2 \theta)^{1/2} - \operatorname{sgn}(\phi)]} e^{ik[(1 + \beta_\infty^2 \tan^2 \theta)^{1/2} - \operatorname{sgn}(\phi)]|\phi|/\beta_\infty^2}. \end{aligned} \quad (4.33)$$

When $\tan \theta$ is $O(1)$, \mathcal{G} can be further expanded for small β_∞^2 to give an expression that will match with the leading-edge ray field when ϕ is positive and that contains the small factor β_∞^3 when ϕ is negative. The transonic approximation had already established that there is no significant radiation upstream of the leading edge, but this subsonic ‘transition solution’ demonstrates that the upstream radiation is $O(\delta)$, which is smaller than all the terms which are being retained in the downstream directivity. As expected of receding waves, the phase term in (4.33) is large, specifically $O(k\delta^{-2/3})$.

5. Outer region

5.1. Leading-edge ray field G_l

We now apply ray theory to the parabolic wave equation (3.5) in order to determine how the sound emitted from the leading edge reaches the far field. We introduce a ‘fast’ variable $\sigma = ik\bar{\sigma}(\phi, \psi)$ for some $\bar{\sigma}$, substitute $G_l = G_l(\phi, \psi; \sigma)$ into (3.5) and set the corresponding equations at each order in k to zero; at $O(k^2)$ this gives the eikonal equation,

$$\begin{aligned} \left(\frac{\partial \bar{\sigma}}{\partial \psi} \right)^2 \frac{\partial^2 G}{\partial \sigma^2} + 2 \frac{\partial \bar{\sigma}}{\partial \phi} \frac{\partial G}{\partial \sigma} - (1 - k_3^2)G &= 2[\beta_\infty^2 - (\gamma + 1)q] \frac{\partial \bar{\sigma}}{\partial \phi} \frac{\partial G}{\partial \sigma} \\ -[\beta_\infty^2 - (\gamma - 1)q]G - [\beta_\infty^2 - (\gamma + 1)q] &\left(\frac{\partial \bar{\sigma}}{\partial \phi} \right)^2 \frac{\partial^2 G}{\partial \sigma^2}, \end{aligned} \quad (5.1)$$

and at $O(k)$ the transport equation,

$$2 \frac{\partial \bar{\sigma}}{\partial \psi} \frac{\partial^2 G}{\partial \sigma \partial \psi} + \frac{\partial^2 \bar{\sigma}}{\partial \psi^2} \frac{\partial G}{\partial \sigma} + 2 \frac{\partial G}{\partial \phi} = O(\delta^{2/3}). \quad (5.2)$$

We have seen in the preceding analysis (see (4.9) with (4.1), for example) that the phase variable $\bar{\sigma}$ must behave like

$$\bar{\sigma} = \psi^2/2\phi + \phi(1 - k_3^2)/2 + O(\delta^{2/3}) \quad (5.3)$$

for sources concentrated near the leading edge. It follows from the transport equation that $G_l = A(\theta)r^{-1/2}e^{ik\bar{\sigma}(\phi,\psi)}$ is a suitable geometric-acoustics description of the flow for some function $A(\theta)$, while examination of the eikonal equation reveals that

$$G_l = \frac{D_l(\theta)H(\phi)}{k^{3/2}\phi^{1/2}} e^{ik[V_1(\theta)\phi + V_2(\theta)\phi'(\phi,\bar{\psi})]}, \quad (5.4)$$

where $D_l(\theta)$ is an arbitrary directivity function and

$$V_1(\theta) = \frac{1}{2}(\tan^2 \theta + 1 - k_3^2) - \frac{1}{8}(\tan^2 \theta + w^2)^2 \beta_\infty^2, \quad (5.5)$$

$$V_2(\theta) = \frac{1}{8}(\gamma + 1)(\tan^2 \theta + w^2)^2 - 1, \quad (5.6)$$

$$w^2 = 1 + k_3^2. \quad (5.7)$$

Some arbitrary constants involved in the calculation of $\bar{\sigma}$ have been set to zero and $A(\theta)r^{-1/2}$ is rewritten as the amplitude given in (5.4) in order to simplify notation. Matching with the inner solution (4.2) now requires that

$$D_l = D_0 + \sum_{j=0}^9 (D_1^j + D_{2c}^j + D_3^j) k^{1-b_j} \delta^{2/3}. \quad (5.8)$$

Given that the above ray field describes downstream-travelling waves and that the acoustic sources are located near the leading edge, it follows that (5.8) is valid for positive ϕ only, as expressed through the step function in (5.4). In the transonic limit there is no upstream radiation, though in the asymptotic analysis in the Mach-wave region we have found that the receding-wave amplitudes are $O(\delta)$ when the local Mach number is less than one.

5.2. Trailing-edge ray field G_t

The trailing-edge ray field is derived in a similar fashion. The same governing equations apply and we assume that the outer expansion of the trailing-edge inner solution displays the same phase. There is an added complication, however, in that the streamline coordinates are discontinuous across the wake sheet of the airfoil; due to the steady circulation, the mean-flow disturbance potential ϕ' has different values above and below the airfoil. The location of the trailing edge in (ϕ, ψ) -space is $(\phi_{\text{TE}}^\pm, \pm 0)$, where $\phi_{\text{TE}}^\pm = 2 + \bar{\phi}' \pm \Gamma/2$. The mean-flow constant $\bar{\phi}'$ is defined as the average of the disturbance potentials above and below the trailing edge,

$$\bar{\phi}' = \frac{1}{2} [\phi'(2, 0^+) + \phi'(2, 0^-)], \quad (5.9)$$

and Γ is the mean-flow circulation around the airfoil normalized by $U_\infty b$. Both $\bar{\phi}'$ and Γ are calculated using the steady TSD code described in §2. Trailing-edge coordinates (ϕ_t, ψ) are defined according to $\phi_t = \phi - \phi_{\text{TE}}^\pm$ for $\psi > 0$ and $\psi < 0$ respectively, and the pair (r_t, θ_t) defines the corresponding polar coordinates. Behind the airfoil, this trailing-edge coordinate system maps continuously to physical space.

The trailing-edge ray field can now be written as

$$G_t = \frac{D_t(\theta_t)H(\phi_t)}{k^2\phi_t^{1/2}} e^{ik[V_1(\theta_t)\phi_t + V_2(\theta_t)\phi'_t(\phi_t, \tilde{\psi})]}. \quad (5.10)$$

The potential ϕ' in the phase distortion of the leading-edge ray field (5.4) is replaced by ϕ'_t for the trailing-edge field (5.10). This is the mean-flow perturbation potential with the arbitrary constant defined such that the potential disappears at the trailing edge, so that

$$\phi'_t(\phi_t, \tilde{\psi}) = \phi'(2 + \phi_t, \tilde{\psi}) - \bar{\phi}' \mp \frac{\Gamma}{2}. \quad (5.11)$$

The ray field (5.10) closely resembles the leading-edge ray field (5.4), though it is expressed in trailing-edge coordinates, has a different directivity function $D_t(\theta_t)$ (to be determined by matching) and, as will be shown in §6, is a factor $O(k^{-1/2})$ smaller.

5.3. Volume-source solution G_p

For an airfoil in subsonic flow, Myers & Kerschen (1995) show that the distribution of volume sources is concentrated near the leading edge where the singularity is responsible for large mean flow gradients, while the sources elsewhere are too small to significantly contribute to the sound generation. However, because in our transonic problem the steady TSD leading-edge singularity is 'stretched' in the transverse direction, the leading-edge analysis assumes a mean-flow singularity that is uniform in Ψ , without decay in the transverse direction (see (2.7)). Although asymptotically correct in region A , the inner solution H_2^j incorrectly predicts plane waves everywhere downstream of the Ψ -axis and a reflection of those waves along the semi-infinite line $\Phi > 0$. Consequently, the outer expansion of this leading-edge solution exhibits singular behaviour (at $\theta = \theta_g$, see (4.21)) that must be resolved by considering the transverse decay of the leading-edge singularity and the finite extent of the airfoil. To this end we examine the particular solution of (3.5) in the outer region.

We first determine the volume-source solution neglecting distortion by the mean flow and interaction with the airfoil, given by the particular solution of

$$\frac{\partial^2 G}{\partial \psi^2} + 2ik \frac{\partial G}{\partial \phi} + k^2(1 - k_3^2)G = 2A_t^* \frac{\partial}{\partial \phi} \{q(\phi, \tilde{\psi})e^{ik\chi(\phi, \psi)}\} \quad (5.12)$$

which disappears when $\phi \rightarrow -\infty$. By Fourier transforming in ψ , solving the resulting ordinary differential equation in ϕ with the upstream boundary condition and applying the inverse Fourier transform, the solution

$$G_p = -\frac{A_t^* e^{\pi i/4}}{(2\pi k)^{1/2}} \int_{-\infty}^{\phi} \int_{-\infty}^{\infty} \frac{(\partial/\partial \xi)\{q(\xi, \tilde{\eta})e^{ik\chi(\xi, \eta)}\}}{(\phi - \xi)^{1/2}} e^{ik\bar{\sigma}_p(\phi, \psi; \xi, \eta)} d\eta d\xi \quad (5.13)$$

is obtained. Here, the double bar across the outer integral denotes finite-part integration, $\bar{\sigma}_p = (1 - k_3^2)(\phi - \xi)/2 + (\psi - \eta)^2/2(\phi - \xi) + O(\delta^{2/3})$ and $\tilde{\eta} = \delta^{1/3}\eta$, analogous to the definition of the coordinate $\tilde{\psi}$. Under the integral signs, we recognise the same leading-order phase terms as those of the ray fields of the previous section (e.g. (5.3)), with ϕ and ψ here replaced by $\phi - \xi$ and $\psi - \eta$ respectively. The same eikonal equation (5.1) then accounts for the ray distortion as represented by the $O(\delta^{2/3})$ phase terms in the solution

$$\bar{\sigma}_p = V_1(\theta_p)(\phi - \xi) + V_2(\theta_p)\phi'_p(\phi, \psi; \xi, \tilde{\eta}), \quad (5.14)$$

where $\tan \theta_p = (\psi - \eta)/(\phi - \xi)$ and

$$\begin{aligned} \phi'_p &= \phi'(\phi, \tilde{\psi}) - \phi'(\xi, \tilde{\eta}) \\ &\quad \times \operatorname{sgn}(\psi) \operatorname{H}(\psi \cot \theta_p) \operatorname{H}(-\eta \cot \theta_p) \operatorname{H}(\xi - \eta \cot \theta_p) \Delta \phi'(\xi - \eta \cot \theta_p). \end{aligned} \quad (5.15)$$

The function $\Delta \phi'(\phi) = \phi'(\phi, 0^+) - \phi'(\phi, 0^-)$ is the jump of the steady disturbance potential across $\psi = 0$. This completes the particular solution G_p , though two clarifying remarks are in order.

First, since the thin-airfoil representation of the mean flow predicts a $|\phi|^{-1/3}$ singularity in q (confirmed by differentiating (2.7) with respect to x), the outer integral in (5.13) diverges, and must therefore be taken in the Hadamard or finite-part sense as denoted by the double bar. This finite part is obtained by taking the derivative with respect to ξ outside the integral after some rearranging, or alternatively by a suitable integration by parts coupled with the assumption that q is continuous everywhere, specifically across $\phi = 0$. This latter interpretation relies on the fact that the actual flow velocity is indeed continuous near the leading edge, and that the local TSD approximation of q merely describes the limiting behaviour of the flow. A more rigorous analysis would recognise the continuous transition between the flows upstream and downstream of the forming Mach wave in an asymptotic region that discerns the stagnation point flow but that provides only an asymptotically small contribution to the sound generation. The expression (5.13) represents the solution in the limit that this region disappears, and its accuracy is confirmed in the leading-edge analysis, where the local approximation of q is used and the resulting expression for G_p can be seen to satisfy conservation of mass, momentum and energy across $\phi = 0$.

The second remark concerns the function ϕ'_p , which is an approximation of the integral $\cos \theta_p \int q dr_p$ that appears when solving the eikonal equation. It is a measure of the phase distortion at the point (ϕ, ψ) for a ray that originates at the source (ξ, η) , which must of course disappear when these two points coincide. The third term of ϕ'_p in (5.15) ensures the continuity of ϕ'_p across $\psi = 0$, as the function ϕ' is discontinuous. The jump of ϕ' across the ϕ -axis is therefore subtracted and the step functions ensure that this occurs if and only if the ray crosses the axis downstream of the leading edge. The argument of $\Delta \phi'$ in (5.15) is $\xi - \eta \cot \theta_p$, which is the ϕ -coordinate of the point where the line joining (ϕ, ψ) and (ξ, η) crosses the axis.

Since the volume sources are not present in the far field, the limit $|\phi|, |\psi| \gg |\xi|, |\eta|$ may be taken in (5.13) to calculate the far-field radiation. By also applying integration by parts as discussed above, the volume-source sound in the far field is found to be

$$G_p \sim \frac{D_p(\theta) \operatorname{H}(\phi)}{k^{3/2} \phi^{1/2}} e^{ik[V_1(\theta)\phi + V_2(\theta)\phi']}, \quad (5.16)$$

where the directivity function D_p is given by

$$D_p(\theta) = k^2 \int_{-\infty}^{\infty} \int_{-\infty}^{\infty} Q(\theta; \xi, \eta) e^{ik[(\tan^2 \theta + w^2)\xi/2 + (k_n - \tan \theta)\eta]} d\eta d\xi, \quad (5.17)$$

and where

$$\begin{aligned} Q(\theta; \xi, \eta) &= \frac{A_t^* e^{-\pi i/4}}{2(2\pi)^{1/2}} (1 - k_3^2 - \tan^2 \theta) q(\xi, \tilde{\eta}) \\ &\quad \times \exp \{ ik [g(\xi, \tilde{\eta}) - g_l + \beta_\infty^2 (w^2 + \tan^2 \theta) (4\eta \tan \theta + w^2 \xi - 3\xi \tan^2 \theta)/8 \\ &\quad - V_2(\theta) \phi'(\xi, \tilde{\eta}) - V_2(\theta) \operatorname{sgn}(\psi) \operatorname{H}(-\eta \cot \theta) \operatorname{H}(\xi - \eta \cot \theta) \Delta \phi'(\xi - \eta \cot \theta)] \}. \end{aligned} \quad (5.18)$$

Noting that the phase in (5.17) varies rapidly with ξ and η when $\tan \theta \neq k_n$, two further integrations by parts are applied to find the leading-order expansion in k of the double integral, leading to

$$D_p \sim \sum_{j \text{ odd}} D_p^j(\theta) k^{1-b_j} \delta^{2/3}, \tan \theta \neq k_n, \quad (5.19)$$

where the functions $D_p^j(\theta)$, given by (4.15), have also been calculated in the inner-region analysis. This far-field result agrees with the form of the scattered-field component of H_{2p}^j , though it does not include the plane-wave and hydrodynamic components given in (4.14).

It is clear that (4.15) and thus (5.19) are not valid near $\tan \theta = k_n$, in which case we must revert to a numerical evaluation of the double integral in (5.17) using computed values of q and ϕ' . (In the examples of §7, we perform the numerical integration when θ lies within 10° of the gust orientation angle θ_g .) For this critical observer angle, D_p is asymptotically larger than (5.19), indicating that the sound is radiated primarily in the direction of the gust orientation angle.

5.4. Complementary solution G_c

The velocity normal to the airfoil now consists of the velocity due to the incident gust, as specified by the right-hand side of the boundary condition (3.8), and that due to G_p . The latter is approximated by differentiating (5.13) under the integral signs, by applying the method of stationary phase for the integral in η and finally by calculating the finite part of the integral in ξ across the Mach wave. The result is

$$\begin{aligned} \left. \frac{\partial G_p}{\partial \psi} \right|_{\psi=0} &= \frac{2k_n A_t^* q(\phi, 0)}{k_n^2 + w^2} e^{ik(\phi + g(\phi, 0^\pm) - g_t)} \\ &+ ik_n H(\phi) \sum_j (-\text{sgn } k_n)^j L_j e^{ik[V_1(\theta_g)\phi - k_n^2\phi + V_2(\theta_g)\phi'(\phi, 0 \text{sgn}(-k_n))]} k^{1-b_j} \delta^{2/3}. \end{aligned} \quad (5.20)$$

The first term in (5.20) is due to the hydrodynamic component of G_p (this component is small in the far field and therefore does not appear in the far-field expansion of G_p) and the second term is due to the (nearly) plane sound wave also found in region A . We write $G_{c,\text{hyd}}$ for the part of the complementary solution that cancels the first term in (5.20) and the velocity of the incident gust, and G_c for the part that cancels the second term in (5.20). Neglecting for the moment the diffraction from the airfoil edges (these are included in G_l and G_t), the former is given by

$$\begin{aligned} G_{c,\text{hyd}} &= \left[A_n + \frac{2k_n A_t^* q(\phi, 0^\pm)}{k_n^2 + w^2} + \frac{A_n q(\phi, 0^\pm)}{w^2} \right] \\ &\times \frac{\text{sgn}(\psi) H(\phi)}{kw} \exp \left\{ \left[-w + \frac{q(\phi, 0^\pm)}{w} \right] k|\psi| + ik\phi + ik[g(\phi, \tilde{\psi}) - g_l] \right\}, \end{aligned} \quad (5.21)$$

valid for $\phi > 0$ and significant in an $O(1/k)$ thick 'hydrodynamic boundary layer' whose extension downstream of the trailing edge ensures that the Kutta condition is satisfied. The accuracy of the result (5.21) is confirmed by substitution into (3.5) and by noting that its derivatives are dominated by derivatives of the phase factors. Clearly, no significant sound is generated along the airfoil away from the edges due to interaction between the hydrodynamic motion and the surface. By contrast, the plane acoustic waves generated by the volume sources are reflected, producing a

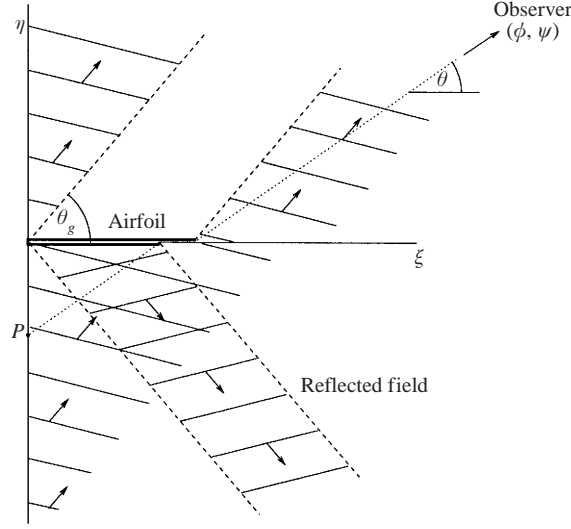


FIGURE 3. Schematic diagram of the plane-wave components of G_p . Plane waves travelling at the gust angle (here assumed positive) are generated in the Mach-wave region all along the η -axis, and are reflected by the airfoil. The origin and the point P define the interval on the η -axis that cannot be seen by an observer at (ϕ, ψ) in the far field.

significant radiation component G_c . (Figure 3 is a schematic representation of the planes waves, their reflection, and the corresponding shadow region, not including the diffracted fields and phase-front distortion.) Again we approach the problem by first determining the solution neglecting any propagation effects due to mean-flow non-uniformities, namely we solve the homogeneous form of (5.12). The solution that is valid in the far field then follows by perturbing the phase such that the eikonal equation is satisfied to $O(\delta^{2/3})$ and the transport equation is satisfied to $O(1)$. The far-field expansion is calculated by taking $r \rightarrow \infty$, and we find a radiation G_c of the form (5.16) with a directivity factor

$$D_c(\theta) = \sum_{j=0}^9 \frac{ik_n L_j e^{\pi i/4} (-\text{sgn } k_n)^j \text{sgn}(\psi)}{(2\pi)^{1/2}} k^{2-b_j} \delta^{2/3} \int_0^{\phi_{TE}^\pm} e^{ik\chi_c^\pm(\theta, \xi)} d\xi, \quad (5.22)$$

where

$$\begin{aligned} \chi_c^\pm(\theta, \xi) = & [V_1(\theta_g) - V_1(\theta) + \tan^2 \theta - k_n^2] \xi - \beta_\infty^2 \tan^2 \theta (\tan^2 \theta + w^2) \xi / 2 \\ & + V_2(\theta_g) \phi'(\xi, 0 \text{sgn}(-k_n)) - V_2(\theta) \phi'(\xi, 0^\pm). \end{aligned} \quad (5.23)$$

The integration is performed along the airfoil surface, and the upper and lower signs are taken when ψ is positive and negative respectively. When $\tan^2 \theta - k_n^2 = O(1)$, an integration by parts shows that, to leading order,

$$D_c(\theta) = \sum_j D_{2c, \sin}^j(\theta) k^{1-b_j} \delta^{2/3} (1 - e^{ik\chi_{TE}^\pm(\theta)}), \quad \tan^2 \theta \neq k_n^2, \quad (5.24)$$

where

$$\chi_{TE}^\pm(\theta) = \partial^\pm(\theta) - \partial^\pm(|\theta_g| \text{sgn } \psi) - \beta_\infty^2 k_n^2 (k_n^2 + w^2) \mp V_2(\theta_g) \text{H}(k_n \psi) \Gamma, \quad (5.25)$$

and

$$\partial^\pm(\theta) = 2V_2(\theta) + [\tan^2 \theta - V_1(\theta) - V_2(\theta)]\phi_{\text{TE}}^\pm - \beta_\infty^2 \tan^2 \theta (\tan^2 \theta + w^2), \quad \cos \theta \neq 0. \quad (5.26)$$

The directivity factors $D_{2c,\sin}^j(\theta)$ are given by (4.21), and $\partial^\pm(\theta)$ is a measure of the acoustic phase shift between the leading and trailing edges. (The analysis of Appendix C will clarify that the expression for this shift is not valid in the Mach-wave region.) The final factor in (5.24), which is not included in the complementary solution of the inner region, accounts for the presence of the trailing edge. Similar to the result for the particular solution, $D_c(\theta)$ is singular in the gust direction, though in this case (4.21) shows that the reflection brings about an additional singularity at $\theta = -\theta_g$. Again, these singularities are avoided by evaluating (5.22) numerically near these critical angles.

6. Other inner regions

6.1. Trailing-edge and transition regions C and D

To determine the directivity function of the trailing-edge ray field (5.10), matching must again be performed. Due to the Kutta condition at the trailing edge, the boundary-layer-type solution (5.21) that extends from the leading edge and continues in the outer region along the length of the airfoil can be taken to also extend past the trailing edge along the wake sheet (Myers & Kerschen 1995). In other words, the convected gust is not diffracted by the trailing edge, and instead the scattered field must cancel the pressure jump across the wake introduced by the leading-edge ray field. The resulting sound is $O(k^{-1/2})$ smaller in amplitude than the leading-edge field. Here, we do not consider the diffraction of the plane-wave component of the particular solution G_p , as this scattering has already been included in the solution G_c (see (5.22)).

The requirement that the pressure be continuous is equivalent to the requirement that the modified pressure \bar{p} , defined by (3.9), is continuous. The jump in \bar{p} across the wake sheet $\varphi = 0$ due to the leading-edge ray field is, from (5.4),

$$\bar{p}|_0^+ = \frac{\Delta_p k^{-1/2}}{(2 + \phi_t)^{1/2}} e^{ik[V_1(0)\phi_t + V_2(0)\phi_t']}, \quad (6.1)$$

where

$$\Delta_p = \frac{iw^2}{2} [D_t(0)e^{-ik\delta^+(0)} - D_t(2\pi)e^{-ik\delta^-(0)}], \quad (6.2)$$

and the phase functions $\delta^\pm(\theta)$ are given by (5.26). At this point it is clear that although the potential ϕ' is small, its influence on the acoustic field is significant due to the large value of k in the expression for Δ_p . In all previous expressions, the $O(\delta^{2/3}k)$ influence of the mean flow on the sound propagation simply resulted in an additional phase factor that does not affect sound power levels, i.e. the amplitude of the unsteady pressure. Due to interference between the leading- and trailing-edge fields, however, the mean flow brings about a potentially $O(1)$ change in the amplitude of the trailing-edge scattered field through the constant Δ_p .

We rescale the governing equation (3.5), this time with local coordinates (Φ_t, Ψ) and corresponding polar form (R_t, θ_t) , defined exactly as in (4.1) but now for the trailing edge. The transformation

$$G_t = k^{-3/2} H_t e^{i(1-k_t^2)\Phi_t/2} \quad (6.3)$$

then leads to the boundary-value problem

$$\frac{\partial^2 H_t}{\partial \Psi^2} + 2i \frac{\partial H_t}{\partial \Phi_t} = 0,$$

$$\frac{iw^2}{2} H_t \Big|_{0^-}^{0^+} - \frac{\partial H_t}{\partial \Phi_t} \Big|_{0^-}^{0^+} = -\frac{\Delta_p}{2^{1/2}}, \quad \Phi_t > 0, \quad (6.4)$$

$$\frac{\partial H_t}{\partial \Psi} \Big|_{0^-}^{0^+} = 0, \quad \Phi_t > 0, \quad (6.5)$$

$$\frac{\partial H_t}{\partial \Psi} = 0, \quad \Phi_t < 0. \quad (6.6)$$

The boundary condition (6.4) specifies the pressure jump in the scattered field required to cancel the pressure jump (6.1) in the leading-edge ray field, (6.5) specifies the continuity of the normal velocity across the wake sheet, and the final condition specifies a zero normal velocity along the airfoil. This problem can be solved exactly using Fourier transforms and the Wiener–Hopf technique (cf., the exact solution for H_0 , equation (4.8)), giving

$$H_t(\Phi_t, \Psi) = -\frac{i\Delta_p \operatorname{sgn}(\Psi) H(\Phi_t) e^{iw^2\Phi_t/2}}{2^{3/2}w^2} \left\{ e^{-w|\Psi|} \operatorname{erfc} \left[\frac{e^{-\pi i/4}(|\Psi| - iw\Phi_t)}{(2\Phi_t)^{1/2}} \right] \right. \\ \left. + e^{w|\Psi|} \operatorname{erfc} \left[\frac{e^{-\pi i/4}(|\Psi| + iw\Phi_t)}{(2\Phi_t)^{1/2}} \right] - 2e^{-iw^2\Phi_t/2} \operatorname{erfc} \left(\frac{e^{-\pi i/4}|\Psi|}{(2\Phi_t)^{1/2}} \right) \right\}, \quad (6.7)$$

and leading to the uniformly-valid outer expansion of the inner solution

$$H_t \sim \frac{D_t(\theta) H(\phi_t) e^{ik\psi^2/2\phi}}{(k\phi_t)^{1/2}} + \frac{i\Delta_p \operatorname{sgn}(\psi)}{2^{1/2}w^2} \operatorname{erfc} \left(\frac{e^{-\pi i/4} k^{1/2} |\psi|}{(2\phi_t)^{1/2}} \right), \quad (6.8)$$

where

$$D_t(\theta_t) = \frac{\Delta_p e^{-\pi i/4} \tan \theta_t}{\pi^{1/2} w^2 (\tan^2 \theta_t + w^2)}. \quad (6.9)$$

The first term in (6.8) corresponds to the trailing-edge ray field, and matches with (5.10) in the outer region. However, the second term in (6.8) does not match with (5.10) when $\psi = O(k^{-1/2})$, and an inner region similar to the transition region of Myers & Kerschen (1995) must be included along the wake sheet (labelled region D in figure 1). This solution accounts for the interaction between rays that pass above the airfoil and those that pass below the airfoil, which experience different distortions according to the difference in the mean-flow properties above and below the airfoil. We treat this region with another set of inner variables, in this case (ϕ_t, η) with $\eta = k^{1/2}\psi$, and look for a solution of the form

$$G_w = k^{-3/2} H_w e^{ik[V_1(0)\phi_t + V_2(0)\phi_t'(\phi_t, 0)]}. \quad (6.10)$$

Here, the boundary-value problem reads

$$\frac{\partial^2 H_w}{\partial \eta^2} + 2i \frac{\partial H_w}{\partial \phi_t} = 0,$$

$$H_w \Big|_{0^-}^{0^+} = \frac{2i\Delta_p}{w^2 (2 + \phi_t)^{1/2}}, \quad \phi_t > 0,$$

$$\begin{aligned}\frac{\partial H_w}{\partial \eta} \Big|_{0^-}^{0^+} &= 0, \quad \phi_t > 0, \\ \frac{\partial H_w}{\partial \eta} &= 0, \quad \phi_t < 0,\end{aligned}$$

and after some considerable calculations the transition solution is found to be

$$\begin{aligned}G_w(\phi_t, \eta) &= \frac{i\Delta_p \operatorname{sgn}(\eta) H(\phi_t)}{w^2 k^{3/2} (\phi_t + 2)^{1/2}} e^{i\eta^2/2(\phi_t+2)} \\ &\times \operatorname{erfc} \left(\frac{e^{-\pi i/4} |\eta|}{(\phi_t(\phi_t + 2))^{1/2}} \right) e^{ik[V_1(0)\phi_t + V_2(0)\phi'_t(\phi_t, 0)]}.\end{aligned}\quad (6.11)$$

This solution is identical in functional form to the leading-order transition solution for the subsonic problem (Myers & Kerschen 1995) apart from the phase factors. The corresponding far-field geometric-acoustics solution is now taken to be of the form (5.10), with D_t replaced by

$$D_w(\theta_t) = \frac{i\Delta_p k^{1/2} \operatorname{sgn}(\psi)}{w^2} e^{-ik \tan^2 \theta_t} \operatorname{erfc}(e^{-\pi i/4} k^{1/2} |\tan \theta_t|). \quad (6.12)$$

This result agrees with the large- ϕ expansion of G_w , it matches with the second term in (6.8), it satisfies the eikonal and transport equations in the outer region, and it is uniformly valid in θ .

6.2. Neglect of region E and shock-wave scattering

The results in §6.1 describe the sound generation near the leading and trailing edges and in the wake transition region D , but calculations involving transition region E on the airfoil surface and for any shock waves have thus far been excluded. We briefly examine these two aspects of the unsteady flow in turn.

First, due to the curvature of the airfoil surface, we might expect creeping waves or whispering-gallery-type solutions to propagate along the airfoil surface, similar to the leading-edge transition solution derived in Myers & Kerschen (1997) for a subsonic, cambered airfoil. The existence of the leading-edge diffracted field ensures that the normal-velocity boundary condition is satisfied in region A , yet this does not imply that its geometric-acoustics representation satisfies the correct boundary condition in the outer region. Taking into account the hydrodynamic boundary-layer solution (5.21) that exists in tandem with the diffracted field and cancels the gust upwash, we require that any additional transition solution cancels the normal velocity on the airfoil surface induced by the leading-edge ray field. This normal velocity is given by the ψ -derivative of (5.4), which is found to be $O(k^{-1/2}\delta)$. Comparison with the calculations in Myers & Kerschen (1997) in the leading-edge transition region reveals that the unsteady potential is then $O(k^{-1}\delta)$ at shallow observer angles θ , and smaller for other polar angles. This is a factor $O(k^{1/2}\delta)$ smaller than the leading-order radiation components, and is therefore negligible compared to the terms retained in the amplitude.

Next, we consider the influence of shock waves on sound generation and propagation, as described in Evers (1999). Previous studies of gust–shock interaction, including Ribner (1953) and Hardy & Atassi (1997), use the Rankine–Hugoniot jump relations to demonstrate that the shock acts to scatter the gust and generate either attenuated or propagating sound waves depending on the mean-flow and gust characteristics. For a normal shock of infinite length with a plane shear wave incident from upstream and

with uniform flow on either side of the shock, the results in Ribner (1953) show that in the transonic limit plane sound waves of amplitude $O(\delta^{2/3}k^{-1})$ propagate downstream of the shock. Although the shock waves in the present study are finite in length and the mean flow is not uniform, Ribner's (1953) analysis can still be applied locally, thanks to the short gust wavelength. Further, in TSD flow shocks are $O(\delta^{-1/3})$ in length, vary in strength on that same scale, and form an angle with the vertical that is $O(\delta^{1/3})$, so that local application of the normal-shock results is certainly justified. Downstream of the shock wave, therefore, the acoustic field (unsteady potential G_s) induced by the gust–shock interaction is governed by the differential equation (3.5) and the boundary condition that is defined by requiring that G_s describes plane waves of appropriate strength at the shock. Naturally, the radiation condition and reflection of waves by the airfoil surface must also be considered in deriving G_s as an integral along the shock length. However, there is no need to perform these calculations here, as it is already clear that the far-field expansion of G_s would lead to a cylindrically decaying sound field with an extra factor $k^{-1/2}$ in the amplitude of the stationary-phase approximation of the integral. This would render G_s an $O(k^{-1/3})$ smaller than the mean-flow effects considered at the leading edge, and it therefore follows that G_s can be neglected.

The sound generation at the shock is similar to the mechanism at the Mach wave extending from the leading edge. Recall that the unsteady flow induced by the gust–Mach wave interaction resembles plane waves at small distances from the leading edge (see (5.20)), yet exhibits the appropriate decay when observed many wavelengths from the source (see (5.16)). Bearing in mind that G_p is asymptotically smaller than its derivatives, (5.20) and (5.16) show that the factor $k^{-1/2}$ separates the order magnitudes of the plane-wave and far-field representations. The significant difference between the mechanisms at the shock and at the Mach wave, however, is that the former is characterized by an $O(\delta^{2/3})$ discontinuity in the mean flow while the latter is driven by a larger $O(\delta^{2/3}k^{1/3})$ discontinuity on the wavelength scale due to the leading-edge singularity.

In addition to the incident gust, the acoustic waves generated at the leading edge interact with the shock wave to generate sound. By the same argument as advanced for the gust–shock interaction, the amplitude of this sound is also asymptotically smaller than the components already considered. However, whereas we are not concerned with how the incident gust is scattered by the shock, some attention must be paid to the refraction of the sound waves. We consider the leading-edge ray field (5.4) and ask whether or not the same expressions are valid downstream of the shock wave. A necessary condition for the unsteady flow to satisfy the shock jump relations is that the phase terms of the upstream and downstream flows are equal across the shock. The same requirement is used by Ribner (1953) and others. Since the mean-flow potential and streamfunction ϕ and ψ are continuous across the shock, and the shock in physical space consequently maps to a single curve in (ϕ, ψ) -space, the exponent in (5.4) must also be continuous across the shock. Therefore, the phase terms of the upstream and downstream flows agree, the same governing equation (3.5) is satisfied, the jump conditions are satisfied to leading order and we therefore conclude that the expressions are valid on both sides of the shock.

7. Results and discussion

7.1. Total far-field solution

The total sound radiated to the far field is written as a sum of ray fields which have been expressed in terms of leading- and trailing-edge coordinates. The scattered field

extending from the trailing edge is now rewritten in terms of the coordinates ϕ and ψ (as opposed to the trailing-edge coordinates ϕ_t and ψ), leading to the additional phase shift $k\delta^\pm(\theta)$ (given by (5.26)). The total far-field radiation is thus given by

$$G_{\text{tot}} \sim \frac{D(\theta)H(\phi)}{k^{3/2}\phi^{1/2}} e^{ik[V_1(\theta)\phi + V_2(\theta)\phi'(\phi, \tilde{y})]}, \quad (7.1)$$

where

$$D(\theta) = D_p(\theta) + D_c(\theta) + D_l(\theta) + [D_t(\theta) + D_w(\theta)] \frac{e^{ik\delta^\pm(\theta)}}{k^{1/2}}. \quad (7.2)$$

The function $D(\theta)$ is the directivity factor of the total geometric-acoustics field, which consists of the following terms. The directivity D_p represents the volume sources near the leading edge, it is dominated by the jump in the anti-symmetric component of the mean flow across the airfoil, and it has a maximum near the gust angle. The deformed plane waves generated by the volume sources are reflected by the airfoil and scattered by the leading and trailing edges, leading to the complementary solution D_c . Scattering of the (distorted) gust and of the hydrodynamic component of the volume-source solution is determined in the leading-edge analysis and is given by

$$D_l = D_0 + \sum_{j=0}^9 (D_1^j + D_{2c}^j + D_3^j) k^{1-b_j} \delta^{2/3}, \quad (7.3)$$

using the expressions (4.9), (4.10), (4.20) and (4.28). The directivity D_0 is the result for a semi-infinite flat plate at zero incidence, while the summation in D_l corresponds to the 10 largest components of the mean-flow distortion brought about by airfoil thickness, camber and angle of attack. The gust distortion by the mean flow leads to the contributions D_1^j , the effects of the volume sources not including those already represented by D_p and D_c are given by D_{2c}^j , and D_3^j are due to the distortion of the flat-plate radiation. A uniform perturbation to the mean-flow speed does not lead directly to the generation of sound, so there is no contribution from H_4 (see §4.5). The leading-edge ray field is rescattered by the trailing edge such that the unsteady Kutta condition is satisfied, resulting in the directivity D_t of (6.9). Not only at the trailing edge, but also further downstream along the wake, the pressure must be continuous and this is realized by the transition solution, and the corresponding directivity D_w is given by (6.12).

For a parametric study of the radiation, (7.1) must be expressed in the physical coordinates (x, y) . Using the far-field approximation (2.6) of the mean-flow TSD solution, ϕ is related to x and $\tilde{y} = \delta^{1/3}y$ by

$$\phi = x - \frac{\Gamma}{2\pi} \tan^{-1} \left(\frac{K^{1/2}\tilde{y}}{x} \right) + \frac{\Gamma + g_l}{2} + O \left(\frac{\log \tilde{r}}{\tilde{r}} \right), \quad (7.4)$$

while the polar angle θ in (ϕ, ψ) -space is also the polar angle $\tan^{-1}(y/x)$ in physical space. The circulation $\Gamma = \phi'(2, 0^+) - \phi'(2, 0^-)$, the average trailing-edge disturbance potential $\bar{\phi}' = [\phi'(2, 0^+) + \phi'(2, 0^-)]/2$, the leading-edge drift g_l , and the parameter η_1 of the leading-edge singularity (see (A 3)) are calculated from the steady TSD code.

7.2. Numerical results

The incident gust is described by eight parameters (A_t , A_n , A_3 , k , k_n , k_3 , B and M_∞), too many for a complete parametric study, so we restrict numerical examples to those excluding entropy gusts ($B = 0$) and gusts with a spanwise velocity component

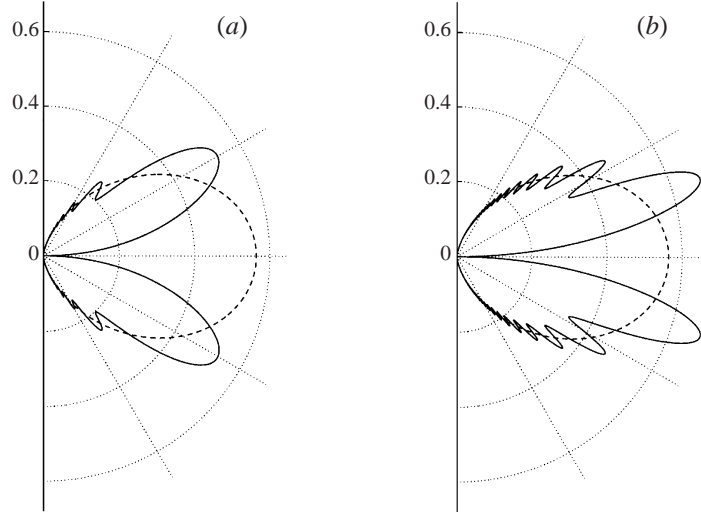


FIGURE 4. (a) Directivity $|D(\theta)|$ for a flat plate with finite chord (solid line) and semi-infinite chord (dashed line) at zero incidence with $k = 5$, $\theta_g = 45^\circ$, $k_3 = 0$ and $M_\infty = 1$. (b) The same flat plate and gust, but with $k = 20$. The mean flow is incident from the left.

($A_3 = 0$). Two further parameters are fixed by the requirements that the gust is solenoidal and has an amplitude of 1 (since the gust amplitude ϵ has already been factored out of the equations), giving the constraints

$$A_t + A_n k_n + A_3 k_3 = 0, \quad \text{and} \quad A_t^2 + A_n^2 + A_3^2 = 1. \quad (7.5)$$

This leaves the four independent parameters k , k_n , k_3 and M_∞ , and we use the gust orientation angle $\theta_g = \arctan k_n$ instead of k_n .

Figure 4 shows the directivity pattern given by $|D(\theta)|$ for a flat plate at zero angle of attack in a stream with $M_\infty = 1$ and for a gust defined by $k_3 = 0$ and $\theta_g = 45^\circ$. In graph 4(a) the reduced frequency is $k = 5$, while 4(b) shows the case $k = 20$, and in both cases the dashed line represents the leading-edge radiation, neglecting trailing-edge rescattering. The rapid oscillations in the total field are due to interference between the leading- and trailing-edge ray fields. The reduced frequency, k , influences the interference patterns through the factor $k^{-1/2} \exp(ik\partial^\pm(\theta))$ multiplying the trailing-edge field. The patterns are dominated by two lobes which contract towards the x -axis for increasing k , and these lobes result from a cancellation of the leading-edge field by the trailing-edge field at shallow observer angles.

When the airfoil is taken to have non-zero thickness and mean loading, the resulting steady distortion influences the far-field intensity through the directivities D_p and D_c (representing the effects of volume sources and reflection by the airfoil surface), through the directivities D_1^j , D_{2c}^j and D_3^j (recall that the part of D_2 corresponding to the source term in (3.5) has been included in D_p) and through an additional phase shift between the leading-edge and trailing-edge ray fields. In figures 5 and 6 we look at the components that make up the total acoustic field for a NACA 0004 profile (4% thickness) at 1° angle of attack in a flow of $M_\infty = 0.9$ and for a gust of reduced frequency $k = 5$, with $\theta_g = 30^\circ$ and $k_3 = 0$. The directivity of the total field is shown by the solid line in figure 5(a) and is compared with the leading-order solution $|D_0|$ (for the semi-infinite flat-plate). The most striking features are the lobes found at the angles $\theta = \pm\theta_g$, similar to those of the previous figure, though with fewer oscillations

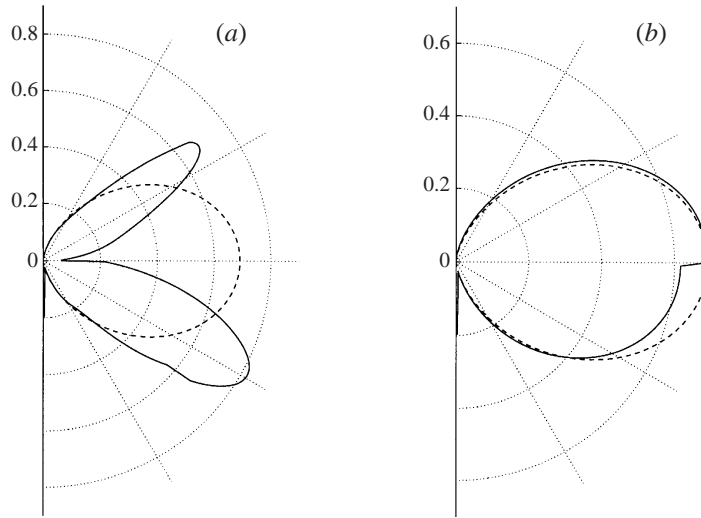


FIGURE 5. (a) The total directivity $|D(\theta)|$ (solid line) and the leading-order directivity $|D_0(\theta)|$ (dashes) for a NACA 0004 profile with 1° angle of attack at $M_\infty = 0.9$. Gust parameters are $k = 5$, $\theta_g = 30^\circ$ and $k_3 = 0$. (b) Directivity of the leading-edge ray field $|D_l(\theta)|$ for the same airfoil and gust (solid line) and again the leading-order contribution (dashes).

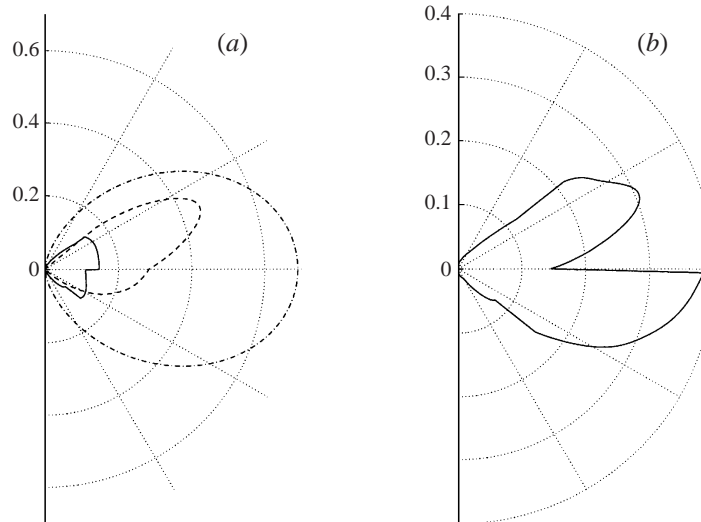


FIGURE 6. (a) The directivity $|D_p(\theta)|$ of the volume-source field (solid line), the directivity $|D_c(\theta)|$ of its reflection (dashes) compared with the leading-order directivity $|D_0(\theta)|$ (dashes and dots), all for the airfoil and gust of figure 5. (b) Directivity $|D_p(\theta) + D_c(\theta)|$ of the volume sources and the corresponding reflection.

because the Mach number is smaller. The lobes are accentuated by the direct and reflected volume-source fields. The leading-edge diffracted field, $|D_l|$, is represented by the solid line of figure 5(b). We note the discontinuity across the wake, due to a difference between the distortion of the leading-edge field above and below the airfoil, and the singular behaviour at steep observer angles, due to the integrable singularity $(\cos \theta)^{2b_j-2}$ of $D_3^j(\theta)$. In figure 6(a), the volume-source solution and its reflection are represented through the plots of $|D_p|$ and $|D_c|$, and a comparison is made with the

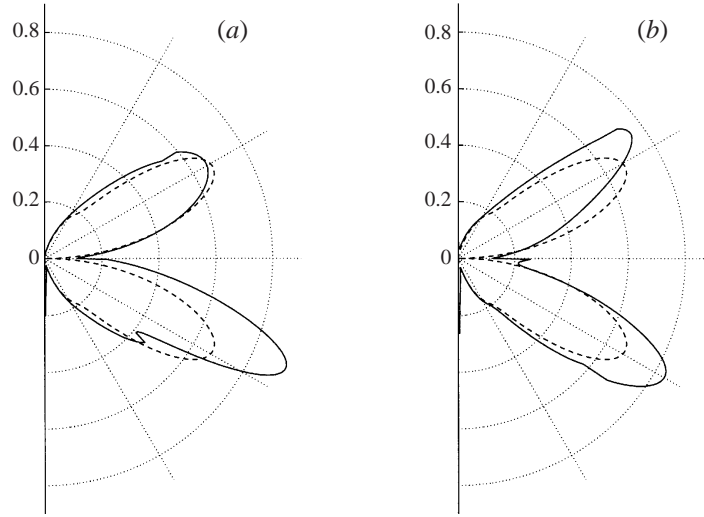


FIGURE 7. (a) Directivity pattern for the airfoil and gust of figures 5 and 6, but with $\theta_g = -30^\circ$ (solid line) and for a flat plate with finite chord at zero incidence with the same gust (dashes). (b) Same, but with $\theta_g = 30^\circ$ and an angle of attack of 2° .

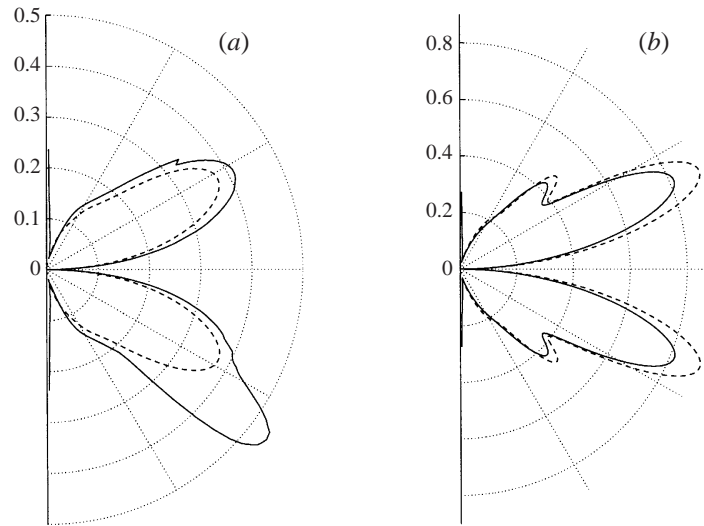


FIGURE 8. (a) Directivity patterns for a NACA 0008 section (solid line) and a flat plate with finite chord (dashes), both at zero angle of attack, with $k = 10$, $\theta_g = -30^\circ$, $k_3 = 1$ and $M_\infty = 0.9$. (b) Same but with $\theta_g = 0^\circ$ and $k_3 = 0$.

same leading-order directivity, $|D_0|$, as in figure 5. The field from the volume sources and the complementary solution combined, $|D_p + D_c|$, is shown in figure 6(b). Due to reflection by the airfoil, this field is slightly stronger below the airfoil than above.

In figure 7(a) the gust angle is taken to be $\theta_g = -30^\circ$ and we see that the lobe in the lower half-plane is even more pronounced. For both positive and negative gust angles, the lower lobe is larger, indicating that a positive angle of attack increases the radiation in the lower half-plane. The gust angle is 30° in figure 7(b), but now the angle of attack is increased to 2° . In both graphs, the total directivity (solid line)

is compared with the directivity for the corresponding flat-plate result (dashes). Even for this very moderate thickness and angle of attack, the influence of the non-uniform mean flow is significant.

We next consider the influence of airfoil thickness on the far-field radiation pattern. Here we take a NACA 0008 airfoil with zero angle of attack and an incident gust with $k = 10$, $\theta_g = -30^\circ$ and $k_3 = 1$ in figure 8(a), and with $k = 10$, $\theta_g = 0^\circ$ and $k_3 = 0$ in figure 8(b). Again, the dashed lines represent the equivalent cases without mean-flow distortion (i.e. a flat plate at zero angle of attack). In the first of the two figures, we find the maximum directivity near the gust angle, whereas the second is symmetric about $\psi = 0$. The comparison with the dashed lines shows that an increase of thickness to 8% of the chord length leads to a considerable increase in radiation when $\theta_g = -30^\circ$, especially in the lower half-plane. By contrast, for the symmetric case $\theta_g = 0$, the increased airfoil thickness leads to a decrease in radiation in both half-planes.

7.3. Acoustic power

An alternative measure of noise levels in the far field is given by the acoustic intensity see (Goldstein 1976)

$$\mathbf{I} = \left(\frac{p'}{\rho_0} + \nabla G' \cdot \mathbf{u}_0 \right) (\rho_0 \nabla G' + \rho' \mathbf{u}_0). \quad (7.6)$$

The energy flux across a circle (at large r) is given by $\mathbf{I} \cdot \hat{\mathbf{r}}$, where $\hat{\mathbf{r}}$ is the unit vector in the radial direction. The time-average of this flux is integrated over $-\pi/2 < \theta < \pi/2$ and divided by $\epsilon^2 \rho_\infty U_\infty^3 b/2$ to formally obtain the normalized radiated sound power as

$$P = \int_{-\pi/2}^{\pi/2} \frac{|D(\theta)|^2}{k \cos^2 \theta} d\theta. \quad (7.7)$$

However, the transonic approximation derived from the parabolic convected wave equation becomes invalid when $\tan \theta = O(\delta^{-1/3})$, as confirmed by analysis in the Mach-wave region, where the subsonic phase of (4.33) replaces the singular transonic phase of (5.4). Consequently, the acoustic intensity is unbounded when $\cos \theta \rightarrow 0$, and the integral (7.7) does not converge. In order to integrate the intensity over the steep observer angles for which the transonic solution is no longer valid, an expression for the eikonal that is uniformly valid in θ is derived in Appendix C.

The normalized acoustic power P , given by the uniformly-valid expression (C 2), is first plotted against the reduced frequency k for NACA 4-digit sections with thicknesses ranging from 0 to 12% of the chord length (figure 9). The radiated power increases with increased thickness, and except for the airfoil with 12% thickness, the radiated power decreases with increasing k . The increase in power with increasing thickness is also evident in figure 10, though here interaction between the leading- and trailing-edge fields leads to a more erratic response to, in this case, changes in the spanwise wavenumber k_3 . At $k_3 = 0$ we note that only a few decibels separate the power levels for the various airfoils, but for $k_3 = 5$ the graphs diverge considerably; even for a moderate airfoil thickness of 4%, the radiated power differs by more than 30 dB from the flat-plate result. This is explained by the fact that the flat-plate solution decays like $1/w^2$ for large $w^2 = 1 + k_3^2$, whereas the additional terms due to mean-flow distortion show weaker or no decay with increasing w^2 . It is interesting to note that although in subsonic flow there is a maximum value of k_3 above which there is no radiation (specifically, there is no radiation from an airfoil in subsonic

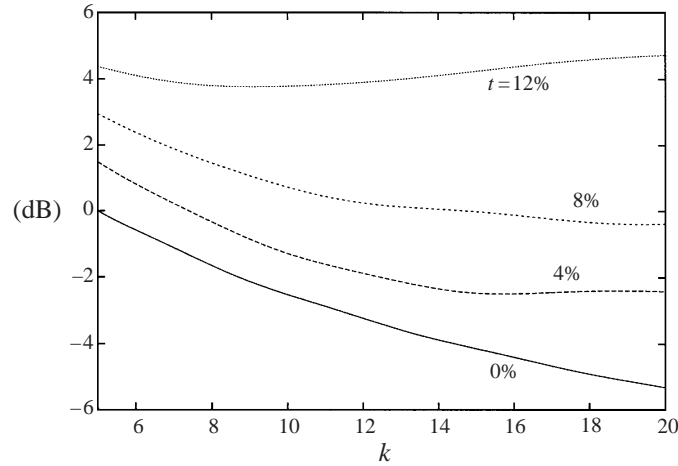


FIGURE 9. Total power in decibels (normalized with respect to the power for $t = 0\%$, $k = 5$) for NACA 00XX sections at zero angle of attack for varying k . Here, $k_3 = 0$, $\theta_g = 30^\circ$ and $M_\infty = 0.9$.

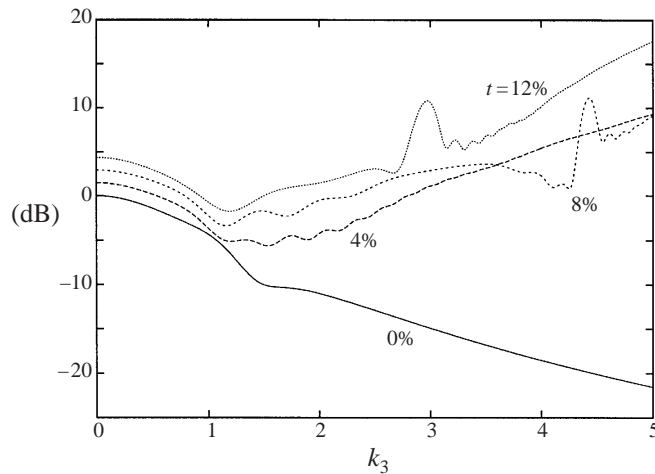


FIGURE 10. Total power in decibels (normalized with respect to the power for $t = 0\%$, $k_3 = 0$) for NACA 00XX sections at zero angle of attack for varying k_3 . Here, $k = 5$, $\theta_g = 30^\circ$ and $M_\infty = 0.9$.

flow when $|k_3| > M_\infty/\beta_\infty$, this is not the case in transonic flow, where radiation is produced for all k_3 .

Finally, we look at the effect of changing the leading-edge radius on the sound power levels of the leading-edge ray field. The thickness of the NACA 00XX section is varied from 0 to 20% of the chord length, the latter corresponding to a nose radius of 4.4%. As in figures 9 and 10, figure 11 indicates an increase in intensity with increased mean-flow distortion. For each of the gust angles considered, the power levels increase by approximately 30 dB.

7.4. Comparison with subsonic theory

The most fundamental similarities between the current work and the subsonic problems of Myers & Kerschen (1995, 1997) and Tsai & Kerschen (1990) are the application of Goldstein's rapid distortion theory and the use of the asymptotic approxima-

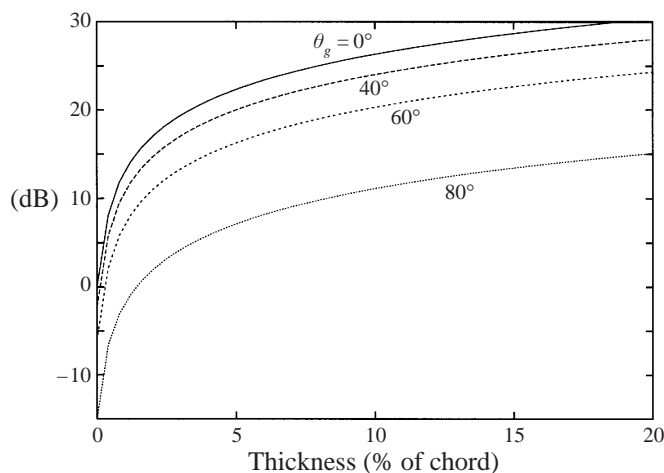


FIGURE 11. Leading-edge power (normalized with respect to the power for $t = 0\%$, $\theta_g = 0^\circ$) for varying airfoil thickness. Here, $k = 10$, $k_3 = 4$, $M_\infty = 1$ and the angle of attack is zero.

tions $\delta \ll 1$ and $k \gg 1$. The procedures used to solve Goldstein's equation that follow naturally from the asymptotics for both the subsonic and transonic cases run parallel in many ways. For instance, the same asymptotic regions near the airfoil leading and trailing edges and along the wake sheet are present in both problems and determine the solution structure; ray fields propagate from the edges, the trailing-edge noise being $O(k^{-1/2})$ smaller in amplitude than the leading-edge noise, and a transition solution that satisfies essentially the same parabolic equation in both cases extends downstream of the trailing edge. A similar asymptotic expansion of the local solution, corresponding to the various interactions between the gust, the mean flow and the airfoil, exists in the leading-edge region. However, the theory does not simply describe the $M_\infty \rightarrow 1$ limit of the subsonic problem which is in fact a singular limit, and it is worthwhile examining the significant differences between the cases $\beta_\infty^2 = O(1)$ and $\beta_\infty = O(\delta^{2/3})$.

Clearly the TSD steady flow about the airfoil is fundamentally different from the subsonic steady flow, and the former is not a limiting case of the latter. The mean-flow perturbation speed accelerates when the oncoming uniform flow approaches the speed of sound, so that $\phi' = O(\delta^{2/3})$, larger than the perturbation potential for subsonic flow. Consequently, the unsteady flow generated by the transonic mean flow–gust interaction is generally $O(\delta^{-1/3})$ larger than for subsonic flow. A second difference between the transonic and subsonic steady flows is the difference between the local approximations of the leading-edge singularity. The subsonic disturbance speed is singular like $(x^2 + \beta_\infty^2 y^2)^{-1/2}$ near the leading edge, while for transonic flow this becomes $|x|^{-1/3}$. Since sound generation occurs on the gust wavelength scale, it follows that the noise due to the various interactions with the mean-flow singularity in the subsonic and transonic cases are $O(k^{1/2}\delta)$ and $O(k^{1/3}\delta^{2/3})$ smaller than the leading-order terms respectively. Although $q = O(\delta^{2/3})$ in steady transonic flow, the disturbance velocity in the y -direction is $O(\delta)$, as dictated by the boundary condition on the airfoil surface, so mean-flow quantities are functions of x alone to leading order. The leading-edge singularity is therefore 'stretched' in the y -direction, indicative of the Mach wave that forms in the transonic limit, and interaction with the gust produces plane sound waves that do not appear in the subsonic solution.

The differences outlined above explain why the transonic problem is not a limiting case of the subsonic problem, though some components of the two sets of solutions do match. For instance, the leading-edge solutions $H_0 + H_4\beta_\infty^2$ represent the $\beta_\infty^2 \rightarrow 0$ expansion of the zeroth-order solution of the subsonic inner-region problem (corresponding to a semi-infinite flat plate at zero incidence). However, this cannot be said of the respective outer expansions nor of the corresponding directivity factors. This stems from the fact that the subsonic problem involves the Prandtl–Glauert coordinates ϕ and $\beta_\infty\psi$, and outer expansions are taken in the limit $\phi^2 + \beta_\infty^2\psi^2 \rightarrow \infty$ as opposed to $\phi^2 + \psi^2 \rightarrow \infty$. Indeed the whole subsonic solution procedure becomes meaningless in the transonic limit because it relies on the Prandtl–Glauert transformation.

The transonic flow described here permits three kinds of discontinuities, the most obvious being shock waves in the mean flow. In addition, the leading-edge singularity stretches below and above the airfoil in the TSD approximation and causes a jump in the disturbance speed q on the wavelength scale, even though a smooth transition that includes the stagnation point exists in the full potential flow. The linearized description is invalid in a region of size $O(\delta^2)$, but this length scale is smaller than the gust wavelength and consequently the unsteady flow experiences the discontinuity only and is unaffected by the transition. Third, the unsteady flow exhibits discontinuous behaviour across $\phi = 0$ in the transonic limit. The jumps in unsteady velocity that result from the parabolic approximation of the mixed-type differential equation are smoothed by local elliptic (or hyperbolic) Mach-wave solutions.

8. Summary and conclusion

The separation of the unsteady parts of the flow from the non-uniform steady base flow and the application of asymptotic techniques involving the parameters k and δ , with the preferred scaling $k\delta^{2/3} = O(1)$, are fundamental to the approach used here to describe high-frequency gust–airfoil interactions. In addition to allowing identification of the relevant physical mechanisms, this approach reduces the problem to smaller manageable ones and lends itself to a blend of different solution techniques, resulting in the combination of a numerical solution of the TSD steady flow and analytical methods for the sound field. We have shown how the different physical processes that determine the sound generation of the airfoil–gust combination are concentrated in a number of asymptotic regions in the flow domain, and how a transonic geometric-acoustics formulation describes acoustic propagation to the far field. The resulting analysis has established the significant components of the radiation field, which are summarized in table 1 along with the orders of magnitude of the corresponding unsteady potentials.

The numerical results of the previous section demonstrate the characteristics of transonic gust–airfoil interaction. The significant features are:

(i) For lifting airfoils, the directivity patterns are characterized by peaks at the gust orientation angle and its reflection. This radiation results from the abrupt change in the strength of the volume sources across the airfoil, which is associated with the steady lift on the airfoil, and therefore does not appear when there is no mean loading.

(ii) The directivity patterns are also characterized by significant interference between the leading- and trailing-edge fields. At leading order, the two fields cancel at the observer angle $\theta = 0$, directly behind the airfoil, resulting in two main lobes on each

Radiation component	Potential	Order of magnitude
Leading-edge diffraction of gust	G_l	$k^{-3/2}$
Trailing-edge rescatter	G_t	k^{-2}
Region D across wake	G_w	k^{-2}
Mean-flow effects at leading edge	G_l	$\delta^{2/3}k^{-1/2-b_j}$
Volume sources in outer region	G_p	$\delta^{2/3}k^{-1/2-b_j}$
Reflection of G_p by airfoil	G_c	$\delta^{2/3}k^{-1/2-b_j}$

TABLE 1. Order of magnitudes of the unsteady potential of the radiated components in the outer region. The 10 constants b_j lie in the range $2/3 \leq b_j < 1$ (see table 2).

side of the airfoil and a series of smaller lobes, the number of which increases with k , at steeper angles.

(iii) As had already been concluded from the analysis, the upstream radiation is negligible and the phase terms of all radiation components are large near the angles $\theta = \pm\pi/2$.

(iv) Mean-flow distortion due to blade geometry and angle of attack may lead to an increase or decrease in radiated energy. When $k = O(\delta^{-2/3})$, the interference effects cause $O(1)$ changes in the total directivity factor.

(v) For increases in the spanwise wavenumber k_3 , the radiation predicted by the flat-plate solution decays faster than additional components attributed to the non-uniform mean flow. Consequently, mean-flow effects account for a greater proportion of the radiation and are increasingly significant for increasing k_3 (note that in the transonic regime, unlike in subsonic flow, there is no cut-off value for k_3 above which the airfoil does not radiate). This is a particularly important result if one were to consider airfoil interaction with highly three-dimensional vorticity.

The work presented here can be extended to describe transonic gust-cascade interaction, a crucial further step in the modelling of turbomachinery noise. Having determined the two expressions for the leading- and trailing-edge ray fields for a single airfoil, infinite rows of such fields will account for the acoustic response by a cascade, though the separate issue of reflections and rescattering by adjacent blades must also be taken into account (see Peake & Kerschen 1997 for the subsonic cascade).

I. E. gratefully acknowledges the financial support provided by the Engineering and Physical Sciences Research Council (EPSRC) and by the European Commission under the Training and Mobility of Researchers (TMR) programme.

Appendix A. Transonic leading-edge singularity

Keyfitz, Melnik & Grossman (1978) show that the perturbation potential ϕ' for TSD flow near a parabolic leading edge can be approximated by a fractional power series in x , and the coefficient and exponent of its leading-order term (and those of higher-order thickness terms) are given numerically. More recently, Rusak (1993) has determined analytically the first two terms including the influence of lift, though the exponents of higher-order terms are only fractionally greater leaving a relatively large approximation error for fixed x . For asymptotic consistency in the unsteady analysis we require the first ten terms.

Our approach is based upon a series solution of the Tricomi equation $\omega\tilde{y}_{\nu\nu} - \tilde{y}_{\omega\omega} = 0$, obtained from the TSD equation (2.2) by transforming to the

hodograph variables

$$\omega = (\gamma + 1) \frac{\partial \varphi'}{\partial x} - K \quad \text{and} \quad v = (\gamma + 1) \frac{\partial \varphi'}{\partial \tilde{y}}. \quad (\text{A } 1)$$

Near the leading edge both ω and v become large and it is convenient to convert to modified polar coordinates ρ and α (or ρ and z) given by

$$\rho^2 = v^2 - \frac{4}{9}\omega^3 \quad \text{and} \quad z = \sin \alpha = \frac{v}{\rho}. \quad (\text{A } 2)$$

(For subsonic flow around a parabolic leading edge ω is negative, $\rho = O(|x|^{-1/2})$ is positive and $z = O(1)$.) The method of separation of variables leads to two families of solutions of the Tricomi equation, one symmetric and the other anti-symmetric in z (see Cole & Cook 1986). Using these solutions, \tilde{y} can be expressed as a fractional power series in ρ :

$$\tilde{y} = \sum_{j=0}^{\infty} \rho^{-\kappa_j} \left\{ \eta_j F\left(\frac{1}{2}\kappa_j, \frac{1}{6} - \frac{1}{2}\kappa_j; \frac{1}{2}; z^2\right) + \mu_j z F\left(\frac{1}{2} + \frac{1}{2}\kappa_j, \frac{2}{3} - \frac{1}{2}\kappa_j; \frac{3}{2}; z^2\right) \right\}, \quad (\text{A } 3)$$

where η_j , μ_j and κ_j are constants and κ_j increase with j . Given the solution (A 3), a similar series

$$x = \sum_{j=0}^{\infty} \rho^{1/3-\kappa_j} \left\{ \eta'_j F\left(\frac{1}{2}\kappa_j - \frac{1}{6}, -\frac{1}{2}\kappa_j; \frac{1}{2}; z^2\right) + \mu'_j z F\left(\frac{1}{3} + \frac{1}{2}\kappa_j, \frac{1}{2} - \frac{1}{2}\kappa_j; \frac{3}{2}; z^2\right) \right\} \quad (\text{A } 4)$$

then expresses the coordinate x in terms of the variables ρ and z . The constants μ'_j and η'_j are related to μ_j and η_j by

$$\mu'_j = \left(\frac{3}{2}\right)^{1/3} \kappa_j \eta_j \quad \text{and} \quad \eta'_j = \left(\frac{3}{2}\right)^{1/3} \left(\frac{1}{3} - \kappa_j\right)^{-1} \mu_j. \quad (\text{A } 5)$$

Finally, the boundary condition (2.3) gives the relation

$$\bar{v} = \pm(\gamma + 1) \left(\frac{R}{2x}\right)^{1/2} + (\gamma + 1)s^{\pm} + o(1), \quad x \downarrow 0 \quad (\text{A } 6)$$

for $v = \bar{v}$ on the airfoil surfaces. On the airfoil ρ is also written as a function of x , $\rho = \bar{\rho}(x)$ say, and by substituting this function and $z = \bar{v}/\bar{\rho}$ into (A 3) and (A 4) with $\tilde{y} = 0$, four relations are obtained, two for each surface. These relations are used to determine the unknowns κ_j , μ_j , η_j and the coefficients and exponents that define $\bar{\rho}$ on each of the two surfaces. Subsequently, ω and thus φ can be determined downstream and upstream of the leading edge. It is not feasible to perform these calculations by hand at higher order, and therefore computer algebra is applied. We note here that the solutions are alternately even and odd, the first one at $j = 0$ being even, and the exponents in (2.7) are $b_j = j\kappa_1/2 + (4 - 7j)/6$, where $\kappa_1 \approx 2.4073$. The coefficients c_j^{\pm} of this series are given by

$$c_j^{\pm} = \eta_1^j \lambda^{-j\kappa_1 + (j+2)/3} (\gamma + 1)^{-1} C_j^{\pm}, \quad \lambda = (\gamma + 1)(R/2)^{1/2}, \quad (\text{A } 7)$$

where C_j^{\pm} are listed in table 2. The constant η_1 cannot be evaluated analytically, as it depends on the circulation around the airfoil which cannot be calculated from a leading-edge analysis, but can formally be determined by matching with the outer flow. Here, the combination $\eta_1 \lambda^{-\kappa_1 + 1/3}$ is approximated numerically using the TSD code described in § 2.

j	C_j^+	C_j^-	b_j
0	-0.600770	2.14782	0.666667
1	-0.893241	0	0.703648
2	0.105101	0.0677791	0.740629
3	-0.208041	0	0.777611
4	0.0413351	0.0400795	0.814592
5	-0.0840239	0	0.851573
6	0.0129519	0.0263838	0.888554
7	-0.0348009	0	0.925536
8	-0.00142637	0.0172927	0.962517
9	-0.0106270	0	0.999498

TABLE 2. Constants defining the series approximation (2.7) of ϕ' .

Appendix B. Mach-wave region

A matching is performed between the solutions in the leading-edge region A and Mach-wave region B (see figure 1) in order to verify the $|\Phi|^{b_j-1}$ singularity of H_{2p}^j for $\Phi \rightarrow 0$, and to determine the eigensolution H_{3e}^j that cancels the $R^{b_j-3/2}$ singularity of H_{3p}^j in the limit $R \downarrow 0$.

The solutions in the leading-edge region A demonstrate that the asymptotics break down in the small- Φ limit when the phase of the scattered field becomes unbounded. Since the solutions $H_{1,2,3}^j$ at the different orders $k^{1-b_j}\delta^{2/3}$ for varying j are independent, we may examine each solution in turn and temporarily set the mean-flow coefficients c_l to zero for all $l \neq j$ for any one of $0 \leq j \leq 9$. The $G_{\phi\phi}$ term in (3.5) is then of the same order of magnitude as $G_{\psi\psi}$ and G_ϕ when ϕ and ψ scale according to

$$\phi = \frac{\varepsilon}{k}\xi, \quad \psi = \frac{\varepsilon^{1/2}}{k}\eta, \quad \varepsilon = k^{(1-b_j)/(2-b_j)}\delta^{2/(6-3b_j)}. \quad (\text{B } 1)$$

This scaling defines the Mach-wave region for each component of the leading-edge field, and the governing equation with $O(1)$ independent variables ξ and η is

$$\begin{aligned} & \frac{\partial^2 \mathcal{G}}{\partial \eta^2} + 2i \frac{\partial \mathcal{G}}{\partial \xi} - b_j c_j^\pm (\gamma + 1) (\text{sgn } \eta)^j \\ & \times \left[|\xi|^{b_j-1} \text{sgn}(\xi) \frac{\partial^2 \mathcal{G}}{\partial \xi^2} + (b_j - 1) |\xi|^{b_j-2} \frac{\partial \mathcal{G}}{\partial \xi} \right] \\ & + (1 - k_3^2) \mathcal{G} \varepsilon + b_j c_j^\pm (\text{sgn } \xi) (\text{sgn } \eta)^j \varepsilon \left[-2 |\xi|^{b_j-1} \frac{\partial^2 \mathcal{G}}{\partial \eta^2} \right. \\ & \left. + i(\gamma - 1)(b_j - 1) \text{sgn}(\xi) |\xi|^{b_j-2} \mathcal{G} + 2i(\gamma - 1) |\xi|^{b_j-1} \frac{\partial \mathcal{G}}{\partial \xi} \right] \\ & = 2A_t^* b_j (b_j - 1) c_j^\pm (\text{sgn } \eta)^j |\xi|^{b_j-2} \varepsilon k^{-1} + O(\mathcal{G} \varepsilon^2, \varepsilon^{3/2} k^{-1}), \end{aligned} \quad (\text{B } 2)$$

where we use \mathcal{G} to denote the unsteady potential in the Mach-wave region. The boundary condition on the positive ξ -axis is

$$\frac{\partial \mathcal{G}}{\partial \eta} = -\frac{\varepsilon^{1/2}}{k} A_n + O(\varepsilon^{3/2} k^{-1}). \quad (\text{B } 3)$$

A particular solution \mathcal{G}_p that satisfies the homogeneous form of the above boundary

condition is found by writing \mathcal{G}_p as a function of ξ alone and by integrating (B 2) at leading order exactly:

$$\mathcal{G}_p = \frac{2\varepsilon A_t^* \operatorname{sgn}(\xi)}{(\gamma + 1)(2 - b_j)k} \exp \left\{ -\frac{\pi i \operatorname{sgn}(\lambda)}{2(2 - b_j)} \right\} |\lambda|^{-1/(2-b_j)} \Gamma \left(\frac{1}{2 - b_j}, i\lambda |\xi|^{2-b_j} \right) e^{i\lambda |\xi|^{2-b_j}}, \quad (\text{B 4})$$

with

$$\lambda = \frac{2(\operatorname{sgn} \eta)^j}{(\gamma + 1)c_j^\pm b_j(2 - b_j)}. \quad (\text{B 5})$$

The large- $|\xi|$ expansion of \mathcal{G}_p is $-ib_j c_j^\pm A_t^* (\operatorname{sgn} \xi)(\operatorname{sgn} \eta)^j |\xi|^{b_j-1} \varepsilon k^{-1}$, and this confirms the singular behaviour of H_{2p} in region A when the Mach-wave region is approached. The result (B 4) demonstrates how the elliptic equation (B 2) can accommodate the continuous transition between the upstream and downstream flows, whereas its transonic approximation predicts a discontinuity. The matching is consistent, and the transonic solution is valid away from the Mach wave.

Next we determine the eigensolution $G_{3e}^j = H_{3e}^j e^{ik(1-k_3^2)\Phi/2}/k$, and to that end we consider the solution of the homogeneous version of (B 2) that satisfies the boundary condition (B 3). This nonlinear problem cannot be solved exactly, but we can determine the outer expansion of \mathcal{G} required for matching with G . The variable \mathcal{G} without any subscript or superscript j is assigned to this solution in the remainder of the Appendix. We use Van Dyke's asymptotic matching principle that $\mathcal{G}^{(m,n)} = G^{(n,m)}$, namely that the $(n+1)$ -term outer expansion of the m th-order approximation of the inner solution \mathcal{G} is equal to the $(m+1)$ -term inner expansion of the n th-order approximation of the outer solution G . Already we know from (4.8), (4.23) and the scaling (B 1) that for $\xi > 0$,

$$\left. \begin{aligned} G^{(0,0)} &= \frac{(\varepsilon \xi)^{1/2} A_n \operatorname{sgn}(\eta)}{k} \left[\left(\frac{2}{\pi} \right)^{1/2} e^{\pi i/4} e^{i\xi^2/2} - |\xi| \operatorname{erfc} \left(\frac{e^{-\pi i/4} |\xi|}{2^{1/2}} \right) \right], \\ G^{(0,1)} &= G^{(0,0)} + \frac{(\varepsilon \xi)^{3/2} A_n \operatorname{sgn}(\eta)}{k} \left[\frac{e^{-\pi i/4}}{3(2\pi)^{1/2}} (w^2 + iw^2 \xi^2 - 6) e^{i\xi^2/2} \right. \\ &\quad \left. - \left(\frac{w^2 |\xi|^3}{6} + i|\xi| \right) \operatorname{erfc} \left(\frac{e^{-\pi i/4} |\xi|}{2^{1/2}} \right) \right], \\ G^{(1,0)} &= G^{(0,0)} + G_{3e}^{(0)} - \frac{\varepsilon^{1/2} (\operatorname{sgn} \eta)^{j+1} E_j}{k} \left(1 + \frac{i\xi^2}{1 - 2b_j} \right) \xi^{b_j-3/2} e^{i\xi^2/2}. \end{aligned} \right\} \quad (\text{B 6})$$

Here, $\zeta = \eta \xi^{-1/2}$ and the term $G_{3e}^{(0)}$ in the third part of (B 6) is the inner expansion of the unknown eigensolution. We postulate that this eigensolution is made up of a linear combination from the complete set of similarity solutions given in Bluman & Cole (1974). With a slight change of variables to conform the solutions from the heat equation to the current leading-order equation $G_\psi \psi + 2iG_\phi + (1 - k_3^2)G = 0$, the only family of similarity solutions from those given in Bluman & Cole (1974) that satisfies the boundary condition $G_\psi|_{\psi=0} = 0$ and exhibits the required singular behaviour for

small R is proportional to $G_E^+ + G_E^-$, where

$$G_E^\pm = \Phi^{b-3/2} (1 + i\tau\Phi)^{1-b} \exp \left\{ \frac{i}{2} (1 - k_3^2) \Phi + \frac{i\Psi^2}{2\Phi} - \frac{i\bar{\zeta}_\pm^2}{2} \right\} \\ \times [C_1 M(\frac{3}{2} - b, \frac{1}{2}, i\bar{\zeta}_\pm^2/2) + C_2 \bar{\zeta}_\pm M(2 - b, \frac{3}{2}, i\bar{\zeta}_\pm^2/2)], \quad (\text{B } 7)$$

M is Kummer's function, the constants C_1 , C_2 , A , τ and b are arbitrary and where

$$\bar{\zeta}_\pm = \frac{\pm\Psi - iA\Phi}{\Phi^{1/2} (1 + i\tau\Phi)^{1/2}} \quad (\text{B } 8)$$

is the similarity variable. Given the singularity that must be cancelled in the limit $R \downarrow 0$, $G_{3e}^{(0)}$ is uniquely determined by expressing (B 7) as a function of ξ and η and expanding in ε . We find

$$G_{3e}^{(0)} = \frac{\varepsilon^{1/2} (\text{sgn } \eta)^{j+1} E_j}{k} \xi^{b_j-3/2} M(\frac{3}{2} - b_j, \frac{1}{2}, i\xi^2/2). \quad (\text{B } 9)$$

The second term of the expansion of G_{3e} depends on the unknown A and τ , and therefore $G^{(1,1)}$ is not yet determined. However, $G^{(1,1)}$ can be fixed by calculating $\mathcal{G}^{(1,1)}$ from $G^{(0,0)}$, $G^{(1,0)}$ and $G^{(0,1)}$ using (B 2), the asymptotic matching principle and the relations (B 6). By comparing the inner- and outer-region equations (B 2) and (3.5), the relation

$$\frac{\partial^2 \mathcal{G}^{(1,1)}}{\partial \eta^2} + 2i \frac{\partial \mathcal{G}^{(1,1)}}{\partial \xi} - b_j c_j^+ (\gamma + 1) (\text{sgn } \eta)^j \xi^{b_j-1} \frac{\partial^2 \mathcal{G}^{(1,0)}}{\partial \xi^2} \\ - b_j (b_j - 1) c_j^+ (\gamma + 1) (\text{sgn } \eta)^j \xi^{b_j-2} \frac{\partial \mathcal{G}^{(1,0)}}{\partial \xi} - 2\varepsilon b_j c_j^+ (\text{sgn } \eta)^j \xi^{b_j-1} \frac{\partial^2 \mathcal{G}^{(0,0)}}{\partial \eta^2} \\ + \varepsilon (1 - k_3^2) \mathcal{G}^{(0,1)} + i\varepsilon (\gamma - 1) b_j (b_j - 1) c_j^+ (\text{sgn } \eta)^j \xi^{b_j-2} \mathcal{G}^{(0,0)} \\ + 2i\varepsilon (\gamma - 1) b_j c_j^+ (\text{sgn } \eta)^j \xi^{b_j-1} \frac{\partial \mathcal{G}^{(0,0)}}{\partial \xi} = 0 \quad (\text{B } 10)$$

can be deduced. Solving for $\mathcal{G}^{(1,1)}$ then gives

$$\mathcal{G}^{(1,1)} = \mathcal{G}^{(1,0)} + \mathcal{G}^{(0,1)} - \mathcal{G}^{(0,0)} \\ + \frac{e^{\pi i/4} c_j^+ A_n \varepsilon^{3/2} \xi^{b_j-1/2} \text{sgn } (\eta)}{8 (2\pi)^{1/2} k} \{ -i(\gamma + 1)(1 - k_3^2) \xi^2 e^{i\xi^2/2} \\ - 2(\gamma + 1)(b_j - \frac{1}{2})(1 - k_3^2) M(\frac{3}{2} - b_j, \frac{1}{2}, \frac{1}{2} i\xi^2) \\ + 2 [8b_j + (\gamma + 1)(b_j + \frac{1}{2})(1 - k_3^2) - 2(\gamma + 1)] e^{i\xi^2/2} \\ - 8(2\pi)^{1/2} e^{-\pi i/4} b_j |\zeta| \text{erfc}(e^{-\pi i/4} |\zeta|/\sqrt{2}) - 8\Gamma(b_j + 1) U(b, \frac{1}{2}, -\frac{1}{2} i\xi^2) e^{i\xi^2/2} \} \\ + \sum_m c'_m \xi^{b'_m} M(-b'_m, \frac{1}{2}, \frac{1}{2} i\xi^2), \quad (\text{B } 11)$$

where the summation represents some linear combination of elementary solutions obtained from $\mathcal{G}_{\eta\eta} + 2i\mathcal{G}_\xi = 0$ by applying separation of variables. The function U is the second confluent hypergeometric function as defined in Abramowitz & Stegun

(1972), and this term cancels the velocity normal to the ξ -axis introduced by the term that involves the complementary error function. It matches with H_{3c}^j , whose inner expansion is calculated by making the simplifying variable transformation that deforms the inversion contour in (4.4) onto the path of steepest descent (without actually employing the method of steepest descent itself, as the exponent is not large but small). The right-hand side of (B 11) is exactly the expression that is obtained when we calculate $G^{(1,1)}$ if and only if A , τ and the constants c'_m are set to zero, and after an inspection of (B 7) with $\tilde{\zeta}_{\pm} = \pm \Psi \Phi^{-1/2}$, we conclude that (4.24) gives the correct eigensolution.

Appendix C. Uniformly-valid phase terms

From (5.4)–(5.6) it is evident that the asymptotic expansion that defines the transonic eikonal becomes disordered when the Mach-wave region is approached, or more precisely, when $\tan \theta = O(\delta^{-1/3})$ and the $V_2(\theta)$ term is of order of magnitude comparable to the $V_1(\theta)$ term. In order that a numerical investigation may still be performed, even at these steep observer angles, we revise our ray-field description of the acoustic radiation as follows.

When $\beta_{\infty}^2 < 0$ and there is no mean-flow distortion ($\delta = 0$), the singularity is resolved by considering the subsonic solution (4.32) that is valid in the Mach-wave region under these conditions. The phase of its far-field expansion (4.33) approximates the term $ik\psi^2/2\phi$ of the transonic phase when $\beta_{\infty}^2 \tan^2 \theta \ll 1$, and we therefore suppose that a uniformly valid expression, $\bar{\sigma}_{\text{uni}}(\phi, \psi)$, resembles the subsonic phase of the Mach-wave region. Indeed, by rescaling the eikonal equation such that $\beta_{\infty}^2 \tan^2 \theta = O(1)$ and substituting the subsonic phase for $\bar{\sigma}$ at leading order, we obtain

$$\begin{aligned} \bar{\sigma}_{\text{uni}}(\phi, \psi) = & (\phi^2 + \beta_{\infty}^2 \psi^2)^{1/2} \left(\frac{1}{\beta_{\infty}^2} - \frac{w^2}{2} - \frac{\beta_{\infty}^2 w^4}{8} \right) - \phi \left(\frac{1}{\beta_{\infty}^2} - 1 \right) \\ & - \frac{\phi'(\phi, \tilde{\psi})(\phi^2 + \beta_{\infty}^2 \psi^2)^{1/2}}{\phi} \left\{ 1 - \frac{(\gamma + 1)}{2} \left[\frac{\phi(1/\beta_{\infty}^2 - w^2/2)}{(\phi^2 + \beta_{\infty}^2 \psi^2)^{1/2}} - \frac{1}{\beta_{\infty}^2} \right]^2 \right\}, \end{aligned} \quad (\text{C } 1)$$

and confirm that it matches (in the limit $\beta_{\infty}^2 \rightarrow 0$) with the phase $V_1(\theta)\phi + V_2(\theta)\phi'$ of (5.4) found earlier. In fact, this eikonal is also valid for all polar angles when there is non-zero mean-flow distortion ($\delta \neq 0$), though only in the far field where $q \ll \beta_{\infty}^2$. The solution of the transport equation is unaffected at leading order, and the ray fields exhibit the same $r^{-1/2}$ decay. Using this uniformly valid expression for the phase, the acoustic intensity is integrable and the normalized sound power is written as

$$P = \int_{-\pi/2}^{\pi/2} \frac{|D(\theta)|^2}{k \cos^2 \theta (1 + \beta_{\infty}^2 \tan^2 \theta)} d\theta. \quad (\text{C } 2)$$

It turns out that the contribution of the radiation in the Mach-wave region to the total acoustic power is asymptotically small.

In order that the integral (C 2) may be computed more easily, the phase shift $\hat{\sigma}^{\pm}(\theta)$ (see (5.26)), which was calculated from the singular eikonal, is replaced by its uniformly-valid equivalent, which is calculated from (C 1). The phase shift between sources at the leading and trailing edges, as observed from the far field (determined

by expanding $\bar{\sigma}_{\text{uni}}(\phi_t, \psi) - \bar{\sigma}_{\text{uni}}(\phi, \psi)$ for large r) is now

$$\begin{aligned} \partial_{\text{uni}}^{\pm}(\theta) = & \phi_{\text{TE}}^{\pm} \left(\frac{1}{\beta_{\infty}^2} - 1 \right) - \frac{\phi_{\text{TE}}^{\pm}}{(1 + \beta_{\infty}^2 \tan^2 \theta)^{1/2}} \left(\frac{1}{\beta_{\infty}^2} - \frac{w^2}{2} - \frac{\beta_{\infty} w^4}{8} \right) \\ & + (\phi_{\text{TE}}^{\pm} - 2)(1 + \beta_{\infty}^2 \tan^2 \theta)^{1/2} \left\{ 1 - \frac{(\gamma + 1)}{2} \left[\frac{1/\beta_{\infty}^2 - w^2/2}{(1 + \beta_{\infty}^2 \tan^2 \theta)^{1/2}} - \frac{1}{\beta_{\infty}^2} \right]^2 \right\}, \end{aligned} \quad (\text{C } 3)$$

which indeed converges to $\partial^{\pm}(\theta)$ when $\beta_{\infty}^2 \tan^2 \theta \rightarrow 0$. To the order considered, this adjustment does not affect the value of the integral (C 2), but since the uniformly valid expression of the phase shift is now proportional to $\tan \theta$, rather than $\tan^4 \theta$, as $\phi \rightarrow 0$, the numerical evaluation of the integral is performed more easily.

REFERENCES

- ABRAMOWITZ, M. & STEGUN, I. A. 1972 *Handbook of Mathematical Functions*. Dover.
- BLUMAN, G. W. & COLE, J. D. 1974 *Similarity Methods for Differential Equations*. Springer.
- COLE, J. D. & COOK, L. P. 1986 *Transonic aerodynamics*. North-Holland.
- ENGQUIST, B. & OSHER, S. 1980 Stable and entropy satisfying approximations for transonic flow calculations. *Maths Comput.* **34**, 45–75.
- EVERS, I. 1999 Gust–shock interaction in transonic small-disturbance flow. *AIAA Paper 99-1972*.
- GOLDSTEIN, M. E. 1976 *Aeroacoustics*. McGraw-Hill.
- GOLDSTEIN, M. E. 1978 Unsteady vortical and entropic disturbances of potential flows round arbitrary obstacles. *J. Fluid Mech.* **89**, 433–468.
- HARDY, B. & ATASSI, H. M. 1997 Interaction of acoustic, entropic and vortical waves with a plane shock. *AIAA Paper 97-1614*.
- HU, H. & KANDIL, O. A. 1994 A hybrid boundary element – finite volume method for unsteady transonic airfoil flows. *Engineering Analysis with Boundary Elements* **14**, 149–157.
- HALL, K. C., CLARK, W. S. & LORENCE, C. B. 1994 A linearized euler analysis of unsteady transonic flows in turbomachinery. *Trans. ASME: J. Turbomachinery* **116**, 477–488.
- KERSCHEN, E. J. & BALSÀ, T. F. 1981 Transformation of the equation governing disturbances of a two-dimensional compressible flow. *AIAA J.* **19**, 1367–1370.
- KERSCHEN, E. J. & MYERS, M. R. 1987 Perfect gas effects in compressible rapid distortion theory. *AIAA J.* **25**, 504–507.
- KEYFITZ, B. L., MELNIK, R. E. & GROSSMAN, B. 1978 An analysis of the leading-edge singularity in transonic small disturbance theory. *Q. J. Mech. Appl. Maths* **31**, 137–155.
- LANDAHL, M. T. 1989 *Unsteady Transonic Flow*. Cambridge University Press.
- LIGHTHILL, M. J. 1952 On sound generated aerodynamically. I. General theory. *Proc. R. Soc. Lond. A* **211**, 564–587.
- MURMAN, E. M. & COLE, J. D. 1971 Calculation of plane steady transonic flows. *AIAA J.* **9**, 114–121.
- MYERS, M. R. & KERSCHEN, E. J. 1995 Influence of incidence angle on sound generation by airfoils interacting with high-frequency gusts. *J. Fluid Mech.* **292**, 271–304.
- MYERS, M. R. & KERSCHEN, E. J. 1997 Influence of camber on sound generation by airfoils interacting with high-frequency gusts. *J. Fluid Mech.* **353**, 221–259.
- PEAKE, N. & KERSCHEN, E. J. 1997 Influence of mean loading on noise generated by the interaction of gusts with a flat-plate cascade: upstream radiation. *J. Fluid Mech.* **347**, 315–346.
- RIBNER, H. S. 1953 Convection of a pattern of vorticity through a shock wave. *NACA Tech. Note* 2864.
- RUSAK, Z. 1993 Transonic flow around the leading edge of a thin airfoil with a parabolic nose. *J. Fluid Mech.* **248**, 1–26.
- SURAMPUDI, S. P. & ADAMCZYK, J. J. 1986 Unsteady transonic flow over cascade blades. *AIAA J.* **24**, 293–302.

- TSAI, C. T. & KERSCHEN, E. J. 1990 Influence of airfoil nose radius on sound generated by gust interactions. *AIAA Paper* 90-3912.
- VERDON, J. M. & CASPAR, J. R. 1984 A linearized unsteady aerodynamic analysis for transonic cascades. *J. Fluid Mech.* **149**, 403–429.